8-2015

DEVELOPMENT AND VALIDATION OF AN OPTICALLY-BASED STRAIN MEASURING ORTHOPAEDIC SCREW FOR FRACTURE FIXATION IMPLANTS

Nakul Ravikumar
Clemson University, nraviku@g.clemson.edu

DEVELOPMENT AND VALIDATION OF AN OPTICALLY-BASED STRAIN MEASURING ORTHOPAEDIC SCREW FOR FRACTURE FIXATION IMPLANTS

A Thesis
Presented to
the Graduate School of
Clemson University

In Partial Fulfillment
of the Requirements for the Degree
Master of Science
Mechanical Engineering

---

by
Nakul Ravikumar
August 2015

Accepted by:
Dr. John DesJardins, Committee Co-Chair
Dr. Joshua Summers, Committee Co-Chair
Dr. Jeffery Anker
Dr. Paul Joseph
Dr. Rodrigo Martinez-Duarte

ABSTRACT

In the USA over 28 million musculoskeletal injuries are treated annually, including 2 million fracture fixation surgeries (about 0.5% of the population).[1] Treatment of large osseous defects use allografts which have failure rates of up to 25%, and complication rates as high as 30-60%.[2] Fracture fixation usually involves mechanical fixation with rods, plates and/or screws which repair slowly and are susceptible to infection. Implant infection and loosening are serious concerns, but can currently only be measured through expensive instrumented implants, biopsy culture, or radiographs. However, none of these directly quantify implant loading and stability. There is therefore a need for a simple, cost effective way to quantify implant loading and stability in patients. The purpose of this study is to develop an optically-based strain measuring orthopaedic screw prototype to quantify strain variation in the implant in-vivo after surgery and monitor the load sharing between the bone and the implant. The screw developed as part of this thesis incorporates a spectral ruler into the screw head, and is based on the Moiré effect which indicates strain. The prototype underwent mechanical testing (cyclic loads ranging from 500 N – 2000 N) to closely resemble in-vivo conditions in order to verify the repeatability and reproducibility of the screw to operate as a measurement system. The screw system developed was able to quantify clinically-relevant bone healing strains in the range of 10-3000 μstrains, corresponding to 0.2 -100 μm change in length for a 5 mm gauge length spectral ruler. A 1500 N load resulted in 68.64% color change of a 100 micron spectral ruler with the screw able to measure load fluctuations as small as 2.17 N. It exhibited good repeatability and reproducibility but also possessed some amount of hysteresis due to the mechanism of the screw. The work presented in this research also gives a brief background on the evolution of screw prototypes

leading to the development of the orthopaedic screw. The findings in this research show encouraging results which will help develop a unique portable tool for physicians to quantify bone healing, implant loosening and/or infection in vivo rather than relying on less quantitative assessments based on pain and radiography. Future research will involve the development of next generation prototypes for orthopaedic screws. It will also look more closely into bending in orthopedic screws and use of luminescent spectral rulers through layers of tissue.

DEDICATION

I dedicate this work to my family for all the encouragement and support throughout and my friends for making me feel at home.

ACKNOWLEDGMENTS

I would first like to thank my advisor, Dr. John DesJardins, for not only his help and guidance with this work, but throughout my masters for making it more of a memorable experience as a member of the Laboratory of Orthopedic Research and Design. I would like to thank Dr. Jeffery Anker, who has been an inspiration and for encouraging me after every single meeting to keep going and never give up. My advisor and committee co-chair from Department of Mechanical Engineering, Dr. Joshua Summers, for helping me out as a career advisor. I would also like to thank my committee members, Dr. Rodrigo Martinez-Duarte and Dr. Paul Joseph for their support and efforts in completing this work. I would like to thank my research partner, Melissa Rogalski for having the patience to literally answer every single one of my questions. I would like to thank Dr. Todd from Mechanical Engineering for lending his equipment for my testing. I had the benefit of many extremely helpful lab colleagues throughout this project as well that I am very thankful for. Thank you to my friends Rahul, Achyut and Vijay, without whom I would be lost. Last but not the least, I would like to thank Matthew and Anna for their efforts in making this thesis look professional.

Study on the luminescent spectral ruler was part of an interdisciplinary team project: Melissa helped by fabricating the strain gages, developing protocols to analyze the reflected color signal and spectroscopic analysis of luminescent signal (e.g. Figure 3. 13, 3. 14, 3. 15, and 3. 16). My work involved designing, fabricating, testing, and analyzing the colorimetric strain indicating screws.

Financial support of the research reported in this thesis was provided by NIGMS of the National Institutes of Health under award number 5P20GM103444-07.

TABLE OF CONTENTS

Page

TABLE OF CONTENTS (CONTINUED) Page

LIST OF TABLES

LIST OF FIGURES

Figure Page

LIST OF FIGURES (CONTINUED) Page

LIST OF FIGURES (CONTINUED) Page

CHAPTER 1

INTRODUCTION

Bone is a specialized tissue that retains the potential for regeneration as it possesses a considerable capacity to repair. It is dynamic in its nature and undergoes continual adaptation by remodeling, which is responsible for growth, integrity, production of blood cells, and mineral homeostasis. Besides these fundamental activities, bone is devoted to vital mechanical functions like support, protection, and movement. It is an ideal tissue for such activities due to its unique mechanical properties like hardness, moderate elasticity, and very limited plasticity and brittleness. They act as insertion points for muscles and for the formation of levers able to make muscles respond. The microstructural arrangements and the presence of cavities in the interior of the bone give it an optimum mass-to-strength ratio.[3] Bone is also a heterogeneous tissue as its composition and structure both vary depending on skeletal site, physiological function, the age and sex of subjects, and the type of vertebrate species whereas the basic components of the tissue are remarkably consistent.[4]

The bone healing, especially from fracture, is a less understood physiologic process and can vary depending on the tissue damage, type of fracture, supporting instrumentation used and many other factors. An ability to monitor the healing process would not only pave the way for a robust treatment but would also help track the load sharing between the bone-implant interface. None of the current methods of non-invasive medical measurement can directly quantify implant loading and stability. Implant infection and loosening are serious concerns, but can presently only be measured through expensive instrumented implants,

biopsy culture, or stress radiographs. Being able to visualize the stress and strain *in-vivo* on the bone-implant interface would provide a significant edge over the current methods of monitoring and treating fracture healing, infection and/or implant failure.

Basic Bone Anatomy and Physiology

The basic components of bone are the bone matrix and the mineral substance. The organic matrix is made up of over 90% type I collagen fibrils and the remaining 10% corresponds to non-collagenous proteins, proteoglycans, and phospholipids whereas the calcium phosphate hydroxyapatite forms the mineral substance of the bone.[3,5] The above mentioned components leads to the formation of bone as a tissue but whole bone, i.e., bone as an organ consists of non-osseous cells, blood vessels, nerve fibers, and bone marrow in addition to the calcified bone matrix and bone cells. The physiological properties of bone are closely dependent on the variable presence of these soft structures, whose relative proportions change with type and age of the bone.

Bone can be categorized into five types based on its shape and the skeletal site as long, short, flat, irregular and sesamoid bones. Long bones have more length than width and are primarily responsible for structural support whereas the short bones have approximately the same length and width and provide support and stability with little movement. On the other hand the flat bones are thin, flat, and curved and provide surface area for protection and muscle attachments. Sesamoid bones are embedded in the tendon and help in the protection of the tendon and increase leverage. A typical long bone structure is made up of diaphysis or the central shaft region which represents the longest part, epiphysis or the two extremities of the bone, metaphysis or the growing portion which lies in between, and the epiphyseal line or

the growth plate located between epiphysis and metaphysis. The macroscopic anatomy of the bone shows that all skeletal segments consist of an outer layer of compact (or cortical bone) and an inner zone (the medulla), which contains bone marrow. The periosteum covers the outer surface of all bones, except the joints of long bones and endosteum covers the inner surface of all bones.

Based on the microscopic appearance there are two types of bones namely: the lamellar bone and the woven bone. The lamellar bone consists of cortical bone which is strong and whose structure is oriented along the lines of stress; and cancellous bone which is more elastic in nature when compared with cortical bone. Cortical bone is dense in structure found in the outside shell or cortex of bones, contributes to 80% of adult skeleton and is more resistant to bending and torsional forces. Cancellous bone is spongy in structure found at the end of long bones, contribute to 20% of adult skeleton and is concentrated at places where compressive forces predominate. Cancellous bone has greater surface area when compared to cortical bone and hence is capable of high metabolic activity. The woven bone consists of immature bone which usually forms the embryonic skeleton and also the fracture callus; and pathologic bone which is randomly organized, weak, and flexible in nature.[6]

The bone connective tissue structure consists of the following types of cells: osteon, Haversian canal, lamellae, lacunae, canaliculi, trabeculae, and Volkmann's canals.[7] The osteon is the functional unit and the Haversian canal carries blood, lymphatics and nerves. The lamellae are concentric plate-like structures that ring Haversian canal and the lacunae are spaces between lamellar rings that house the osteocytes. The canaliculi are small canals for transmitting nutrients and cell signals, trabeculae are unit components of the cancellous bone,

and Volkmann's canals connect the Haversian systems to endosteum and periosteum. Among the above cells the main bone cells are namely: osteoblasts, osteoclasts, osteocytes, and osteoprogenitor cells. Some of the growth factors that control cell proliferation, differentiation and survival are Bone morphogenetic proteins (BMPs), Insulin-like growth factors (IGFs), and Cytokines like Interleukin-1 (IL-1), interleukin-6 (IL-6), and tumor necrosis factor (TNF).[8]

The mesenchymal cells and the hematopoietic cells found in the bone marrow are the two types of osteoprogenitor cells which give rise to osteoblasts. Osteoblasts are non-mineralized organic components of the bone matrix which initiate and control mineralization of osteoid material. They produce pro-α 1 collagen (a major component of osteoid), osteocalcin, and bone morphogenic proteins. Osteocytes comprise 90% of all the cells in the mature skeleton.[3] They maintain the bone and are capable of bone formation and resorption. They also play a vital role in controlling extracellular concentration of calcium and phosphate. The osteoclasts are responsible for breaking down the bone matrix, bone resorption and removal.

Bone Biomechanics

The biomechanical performance of bone is limited by its material and structural properties which can be measured by testing whole anatomical units or smaller specimens prepared to isolate particular material components. With this background, the fracture of bone can represent failure of the whole bone at the structural level and bone tissue at the material level.[3] In normal physiological situations, the mechanical behavior of the bone can be compared to that of an elastic material with no visible change in external appearance. Bone has the ability to retain its morphological features for an indefinite period of time even after

degrading. Bone has an adaptive mechanism unlike inorganic materials to respond to increased or decreased function by giving tissue the ability to repair itself, altering its mechanical properties and morphology.

The primary biomechanical purposes of fracture fixation are to deliver stability during healing, to preserve axial and rotational alignment, and to offer load sharing or offloading until the conclusion of fracture healing. The primary objective of the fracture fixation device is to support load, while the secondary objective is to provide an optimum strength and stiffness that enables bone healing to occur. The latter objective is very tough to achieve due to the fact that incorrect implant strength and stiffness can shield the bone from stresses that are required for healing and remodeling.[9] According to Wolff's law the stress shielding or unloading of bone causes bone loss near bone-implant interface.[10]

With respect to screw implantation, the tissue immediately adjacent to a screw may undergo necrosis and absorb due to initial trauma of inserting the screw. The tissue ingrowth into the threads occur once the screw is firmly fixed into the bone. Weight bearing should be prevented until firm fixation has occurred to prevent micromotion between screw and surrounding bone as this will lead to fibrous capsule formation at interface. Perren[11,12] describes in his review that increased contact surface results in increased porosity ultimately leading to blood supply damage. Through this it can be predicted that there is a relation between internal remodeling and necrosis as it results in porosity in the site of necrotic bone.[13] The necrosis may lead to infection at the site of bone-implant interface and hence the goal must be to decrease the area of necrosis and to separate the area of contact between each other.[11] As discussed earlier, bone is a nonlinear, viscoelastic, anisotropic, and heterogeneous

material which makes it very complex to analyze mechanically. It gets even more complex with its fundamental ability to adapt continuously to metabolic and environmental changes in-vivo which further limits the understanding of specific bony mechanics.[14]

Bone Fracture and Healing

Bone fracture occurs when external forces exerted on the bone produce localized stresses in the bone that exceed its specific material properties. If bones experience diseased conditions like cancer or osteoporosis, these material properties decrease and can result in a higher chance of fracture. Bone susceptibility to fracture is related to its energy-absorbing capacity and modulus of elasticity. The former is affected by the rate of loading i.e., rapidly loaded bone will absorb more energy than when loaded at a slower rate. The energy absorbed by the bone during loading is released when the bone fractures.

Bone fractures can be classified into many different types based on loading, anatomy and energy, among others. One of those classification is based on the type of external force exerted namely: Tensile forces lead to transverse fracture, compressive forces lead to oblique fractures, bending forces lead to butterfly fracture and torsional forces lead to spiral fractures.[3,15] But the three general types are Simple, Compound and Comminuted fractures. In simple fractures the bone breaks cleanly without penetrating the skin whereas the bone protrudes through the soft tissue and the skin in the case of compound fractures. The latter is harder to treat and may result in severe infection. The bone fragments into many pieces in a comminuted fracture and this is more common in high energy fractures or in the elderly, whose bones are more brittle.

The endosteal and periosteal blood supply are disrupted due to initial trauma and the fracture site requires adequate blood supply which is essential for bone healing.[16] Bone repair can be described by the following five steps: fracture hematoma or clot formation, internal and external callus formation, removal of bone fragments, formation of new bone from cartilage by osteoblasts present in periosteum, and swelling at fracture followed by remodeling.

There are four classic stages of natural bone repair. Inflammation or hematoma formation is the first stage and lasts for about four to seven days. In this stage the inflammation clinically appears as swelling, pain, erythema, and heat. The torn blood vessels hemorrhage and a mass of clotted blood forms at the fracture site. This is prompted by the migration of inflammatory cells, which stimulate angiogenesis and cell proliferation. The second stage is soft callus formation and it goes on for about two weeks. Granulation tissue (soft callus) forms a few days after fracture, which begins with the infiltration of fibrous tissue and chondroblasts surrounding the fracture site. The capillaries grow into the tissue and phagocytic cells begin cleaning debris. Osteoblasts and fibroblasts migrate to the fracture and start reconstructing the bone. The bone ends are connected by the collagen fibers which are secreted by the fibroblasts. The formation of the spongy bone occurs with the help of osteoblasts and an external bulging cartilaginous matrix is also secreted by the osteoblasts furthest from the capillaries. The matrix calcifies later and the structural network formed adds stability to the fracture site.[17]

The third stage is hard callus formation where the new bone trabeculae appear in the fibrocartilaginous callus. The soft callus is then converted into rigid bone by endochondral ossification and intramembranous bone formation. The bone callus begins three to four weeks

after injury, and continues until firm union is formed two to three months later. Once the fracture has united, bone remodeling which is the fourth and the final stage begins and can last for about a year or even up to four years. The excess material in the medullary canal and on the bone shaft exterior is removed. The lamellar bone replaces the fibrous bone and the compact bone is laid down to reconstruct shaft walls.[17] This process of bone repair is also known as secondary bone union or indirection fracture repair. It is the natural and expected way that fractures heal, and is less rigid in that it has relative stability and flexibility.[3,4]

The basic components of bone which is a heterogeneous tissue, are assembled in different ways with the main structural determinants being age, the type of bone, loads, and metabolic activity. The architecture of the bone is maintained by the mechanical functions acting on the bone whereas the metabolic activities are responsible for the renewal. Both mechanical functions and metabolic activities are due to various aspects of bone remodeling, which induces the erosion and reconstruction of trabecular segments in spongy bone, and of osteons and other lamellar structures in compact bone.[10,18,19]

Fractures which have less than an anatomic reduction and less rigidity heal with callus formation or secondary healing with progression through several different tissue types and eventual remodeling. These have large fracture gaps and low strain and are treated via external fixation, casting and intramedullary [IM] nailing. On the other hand, fractures with no gap have low strain and result in primary healing (cutting cone) without production of callus. These are usually treated via open reduction and internal fixation using interfragmental compression and plating. Internal fixation of a fracture by anatomic reduction and absolute stabilization, alter the biology of fracture healing by diminishing strain (elongation force) on the healing

tissue at the fracture site.[16] This type of bone healing is known as direct bone healing or primary bone union and essentially, the process of bone remodeling allows bone to respond to the stresses to which it is exposed. In this type, the osteons which reach the fracture cross it where bone-to-bone contact exists and unite to bridge the gap by interdigitation. Then the membranous bone fills the small gap between fragments and remodels into cortical bone. This happens as long as the strain applied to these tissues does not cause excessive disruption and fibrous tissue develops (non-union).[15]

Lack of deforming bulky callus, rapid rate of maturation and remodeling, early resumption of rehabilitation and function, and accurate anatomic function are some of the advantages of union with a fixation device. The disadvantages are the inability to accurately determine when union has occurred radiographically due to the absence of peripheral callus, absence of external callus inclining to re-fracture after early union, and stress shielding[11] of bone beneath the fixation device.[20] When the fixation fails it leads to non-union and there are two types namely: fibrous no-union and cartilaginous non-union. The former is due to the interposition of mature fibrous tissue in fracture gap and lack of osteoid and new bone in the callus whereas the latter is due to the formation of cleft lined by fibrocartilage with surrounding capsule. Non-union is very difficult to treat as it persists indefinitely once it is well established. Some treatment methods are either by excision and re-apposition with shortening, replacement by an intercalary graft, or by-pacing the non-union with a bone graft.[21]

The main factors affecting fracture healing are as follows: the energy transfer of the injury, the tissue response which is based on the ends of the bone in opposition or compression, micro-movement or no movement, infection or no infection, the patient, and

the method of treatment. Successful fixation is often influenced by the type of the bone, degree of immobilization, extent of local necrosis, soft tissue damage, presence or absence of infection, and other general systemic factors.

Orthopaedic Fracture Treatment Options

Historically fractures have been treated with immobilization, traction, amputation, and fixation devices. Immobilization is usually treated for long bone fractures using casting, bracing and splinting whereas traction treatment involves the use of pins and wires to hold the bone in place. Compound fractures and ballistic wounds with long fractures which are not amendable to standard fracture care result in amputation due to the associated soft tissue injury and the difficulty of preventing sepsis. Fixation devices like plates, screws, rods, and wires can be both external and internal depending on the type of fracture. Although internal[22] fixation is more widely used due to less infection rate, external fixation may be needed for severe comminuted fractures.[16] External[23] fixators which are placed outside the skin are mainly used to stabilize the bone fragments. Internal fixators work on the standard of load sharing either static or cyclic which either applied through compression or torsion and offer sustenance until the bone is entirely rehabilitated.[14] The most important goal of fracture treatment is to avoid non-union and maintain mechanical stability. Apart from that it aims at restoring the patient to optimal functional state, prevent fracture and soft-tissue complications, and to rehabilitate the patient as early as possible.

Casting treatment is mainly used for stable, closed and aligned fractures. For fractures which are complicated and not able to realign by casting, open reduction and internal fixation is used. Open reduction and external fixation is generally applied to complex fractures that

cannot be repaired using internal fixation. Some of the commonly used fixation devices are wires, pins, screws, and plates. Wires are the simplest and the most versatile implants used to hold fragments of bone or shattered bone together. Pins are wires which have diameters greater than 3/32 inch and are used where plating is difficult to achieve stability.[16] Screws are mainly used to connect bone fragments individually or in conjunction with plates and can convert the torsional load into axial compression load between the head of the screw and the bone. Direct mechanical stability in internal fixation is achieved by means of plates. They vary based on screw placement and cross-sectional shape and can possess different structural properties.

Screws are the most widely used fracture fixation devices and are defined based on inner root diameter, outer diameter, pitch and thread density, type of thread, and type of tip. The inner root diameter determines the strength of the screw and it is the lower extreme diameter of the thread. The outer diameter is the larger extreme diameter of the thread and pitch is the vertical distance between the threads. The threads can be either V-shaped threads or buttress threads and the screw tips can be either self-tapping which cuts its own threads during insertion or non-self-tapping which generally requires a pre-drilled hole.

There are various types of orthopaedic screws depending on the type of fixation required. Cortical screws are mainly used for cortical bone applications and have threads on all shaft length. Cancellous screws are normally used for cancellous bone applications and have threads only on the distal part of the shaft. Both of these screw types can be used as lag screws. It is a technique whereby a screw can produce compression between two objects: the screw thread must grip only the distal fragment and the portion of the screw in proximal fragment

must be free to glide as screw tightens. Cannulated screws are basically hollow screws which provide initial placement of guide wire to assess screw orientation before insertion, thus avoiding screw removal and repositioning. They generally have a larger inner diameter than non-cannulated screws, increased root diameter which helps to maintain screw strength, and relatively smaller thread width which results in lower pull-out strength.[21]

Screw pull-out strength is an important factor that needs to be considered during fixation. When more volume of the bone caught between threads, the pull-out strength will be much greater. Higher pull-out strength can also be achieved by increasing the number of threads in contact with the bone or by increasing the width of the screw thread. Both cortical and cancellous screw types possess almost equal pull-out strength assuming similarly sized design features. By increasing the inner root diameter, the screw strength increases and also the resistance to fatigue failure. Other parameters which increase the pull-out strength are increasing the outer diameter, decreasing the inner diameter, increasing the thread density, and increasing the thickness of the cortex. During implantation, to minimize stress concentrations at the junction of the head and shaft, the screws should be countersunk into a bone or plate. There are also chances of corrosion or failure of the screw after implantation due to improper positioning. Depending on the surgeon, patient, application, and material used the screws may be removed or left in place following fracture healing.[16]

The Role of Strain in Bone Physiology, Fracture and Healing

There are many combinations of plates and screws that can be used depending on the type, location and severity of the fracture in order to obtain the right balance of strength and elasticity (or structural stiffness). An axial tension is generated through a screw when the head

of the screw comes in contact with the cortex or fixation device which causes the bone fragments to compress and maintain stability. Orthopaedic screws usually generate up to 3000 N of compressive force depending on the fracture site and decreases as the bone is remodeled to the stress. Generally, before substantial loss of compression occurs, the fracture healing process is completed.[16]

Bone is stronger in compression, weaker in tension, and weakest in shear. So when subjected to bending forces the convex side of the bone is under tension and the concave side is under compression, resulting in the convex side failing first. By bending a compression plate, the tension side of the eccentrically loaded bone is compressed across the whole fracture. A max force of about 600 N is generally applied which provides absolute stability for two-part fracture patterns and is typically used for simple fractures which do not require lag screws. With these orthopaedic plates having the ability to display strain, it would help clinicians to monitor the fracture gap strain throughout the healing process.

Apart from monitoring implant loosening and infection through the orthopaedic screw, measuring strain would be complimentary. The in-vivo strain on the bone can be studied using the Interfragmentary strain model by Perren[11] and experimental work by Comiskey[24]. Interfragmentary strain is defined as the relative displacement of fracture gap ends divided by the initial fracture gap width. If the tissues experience strain beyond their ultimate strain then they cannot form in the fracture gap.

$$\varepsilon_{gap} = \frac{Fracture\ Gap\ Displacement}{Initial\ Gap\ Width} \Rightarrow \frac{\Delta u}{L}$$

He showed that when this ratio is less than 2% then there is bone formation and primary fracture healing will occur. When the ratio is between 2% and 10% then fibrocartilage formation occurs and the fracture will heal by secondary healing. If the ratio is beyond 10% it leads to the formation of granulation tissue which results in fracture of the fracture gap callus and non-union will occur.[25] As the tissues form in the fracture gap, they stiffen the fracture gap and this in turn leads to lower strains, which allows formation of next stiffest tissue and this cycle repeats until all bone is formed. Summarizing the fracture healing, it shows that immobilization favors differentiation into osteoblasts, motion favors differentiation into chondroblasts, and tensile stress favors differentiation into fibroblasts.

Current Methods to Measure Strain In Vitro and In Vivo

The mechanical behavior of the bone can be compared to that of an elastic material with no visible change in external appearance. One of the most fundamental concepts from the study of mechanics of materials is the relationship between stress and strain. To characterize the material properties like modulus of elasticity of a material, one can apply known loads and measure the normal strain or the deformation per unit length in the material.[3] The earlier strain measuring devices were mechanical in nature and nowadays make use of both optical methods and electrical devices. Based on the type of measurements, the methods are classified into either full-field or point measurements.

The full-field methods can be further classified into methods based on grids and rulings, photoelasticity, and optical interferometry. The method based on grids and rulings gives visual confirmation of displacement change which when divided by the original length, gives the resulting strain. This is effective only at large scale changes and the accuracy of which

is limited to markings on or around the test specimen. Photoelasticity[26] is an experimental method based on the property of double refraction, a property where a ray of light passing through a material experiences two refractive indices. It is used to determine the stress distribution in a material at critical points of irregular geometries and it comes into play typically when mathematical methods become extremely complex. Photoelasticity materials exhibit double refraction when stresses are applied on them and the magnitude of the refraction indices at each point in the material is directly related to the state of stresses at that point. A polariscope is used to calculate the maximum shear stress and its orientation by analyzing the double refraction.[26] Optical interferometry works on the principles of constructive and destructive interference of light so as to produce alternating light and dark bands.[27] This method is widely used to measure small displacements and surface irregularities, and higher sensitivity is achieved by combining it with the moiré effect. When two similar arrays of equally spaced lines or dots are arranged in such a way that one array can be viewed through the other, moiré effect occurs and the dark and light bands which form the interference are known as moiré fringes.[28–30] Large scale changes are seen in the moiré pattern when there is only slight motion of one of the objects. Although these two methods are used for many industrial applications, all of the instrumentation and the requirement of a photoelastic material inhibits these techniques from being used for calculation of in-vivo implant stress distributions.

Point measurement methods can be further classified into clip-on extensometers and bonded electrical resistance strain gauges. Clip-on extensometers can accurately measure deformation in a defined section of a test specimen and are used where high precision strain

measurements are required. Even though they have advantages like low cost and ease of attachment and removal, they are prone to cause stress concentrations at contact points and damage delicate samples. Bonded resistance strain gauges[31,32] consist of a grid of thin metallic foil bonded to a thin insulating backing. The backing is attached to the test specimen with a cyanoacrylate adhesive which helps in transmitting the strain on the surface on to the grid and the electrical resistance of this grid material varies linearly with strain. The change in the electrical resistance of the grid material measures the strain in the specimen. It is small in terms of size and mass, low in cost, can be made of various gauge lengths, moderately affected by temperature changes, and has high sensitivity to both static and dynamic strains.[33] Both these point measurement devices require transdermal wires in order to measure the change in strain, which provide a site for infection to possibly occur. Currently, the methods being used to measure in-vivo strain include ultrasound of liquid filled cavities,[34,35] strain gauges cemented onto bone or devices, and wireless systems that use telemetry. These devices are limited by the need for large data acquisition devices, unsuitable for non-invasive use, and the increased risk of infection. It is evident that none of these have the ability to directly quantify the stability or loading of an implant in-vivo after surgery. Therefore there is a need to develop a system with the ability to non-invasively track the strain on orthopedic devices implanted in tissue and help physicians to be able to quantify implant stability and loading in patients.

To address this need, a spectral ruler was developed through this research which works on the principle of luminescence and moiré fringe pattern. Luminescence works on the principle that when an energy source causes electron atoms to transfer out of their lowest energy "ground" state into a higher energy "excited" state, the electron returns the energy in

the form of light in order to return to its "ground" state.[36] This technique will be used through tissue and the emitted light will be captured through a spectroscope and analyzed.[37] The strain on the orthopaedic screw will cause the moiré fringes to shift, therefore revealing more of one color and less of the other. We hypothesize that these measurements will provide quantitative thresholds for safe load-bearing and early indication of pathologies such as non-union and infection. This research presented is an introduction to a unique optical in-vivo strain measuring technique on implants. It primarily describes the development of a novel strain-indicating orthopaedic screw which will be capable of non-invasively monitoring pre-tension and load sharing with the developing fracture callus. In addition, it also focuses on the mechanical side of things, describing the prototyping and the incremental screw designs in the form of a case study.

The primary requirements where extracted from the problem statement and the first prototype was designed. The limitations that emerged from the prototype test results were further recognized as secondary requirements or as opportunities to improve the design for the successive prototypes. The design changes that emanated were implemented accordingly.

1. The screw must have a geometrical bounding box so as to incorporate the mechanism inside the screw head.
2. The material of the screw must be biocompatible.
3. The screw should possess the ability to be fastened easily.
4. A mechanism to translate the longitudinal elongation of the screw in terms of color change in the spectral ruler.
5. The mechanism should be able to detect micro strains on the screw.

CHAPTER 2

DEVELOPMENT OF SCREW PROTOTYPES

MATERIALS

Spectral Ruler

The spectral ruler consists of a sheet of alternating white and magenta colored lines overlaid with a transparent sheet containing alternating black lines and transparent spaces as shown in Figure 2. 1. This is based on the concept of Moiré's fringe interference pattern formed by two sets of parallel lines, superimposed with one another and/or one set inclined at an angle of 5º to the other. Patterns were printed on white paper for sheet with magenta lines and on transparent film for sheet with black lines using an Epson Stylus Photo R200 ink jet printer (Long Beach, CA); the printed lines are 100 microns in width. In order to measure strain through tissue, the spectral rulers will be modified to incorporate luminescent materials. Relative horizontal motion between the two sheets produces a change in color visible through the transparent spaces. The two sheets must be in contact with each other in order to achieve angular independency while viewing. The requirement was for a screw mechanism to achieve a relative displacement between the two layers of the spectral ruler.

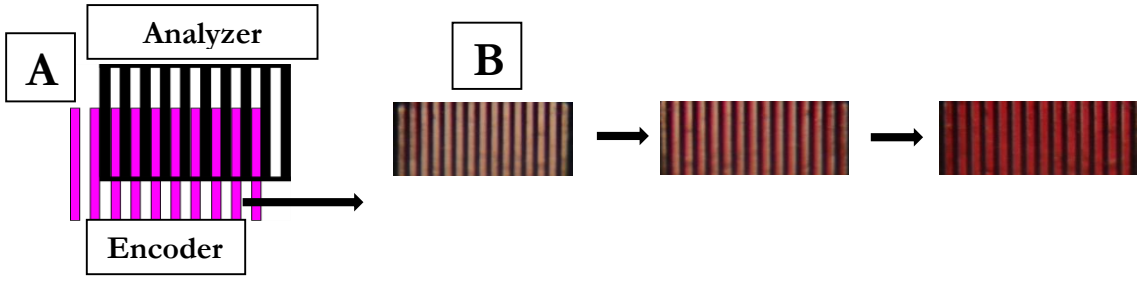

Figure 2. 1: Spectral ruler principle. A) Schematic: an analyzer mask overlays on a patterned encoder, B) Images of spectral ruler from screw elongation during testing.

EVOLUTION OF SCREW PROTOTYPES

This section gives a brief background on the evolution of screw prototypes. Each prototype is elucidated in terms of its design, working, testing and results. It acts as a road map showing the design changes that the various screw prototypes underwent leading to the development of a clinically used orthopaedic screw. Most part of the work on prototype 1 and prototype 2 were carried out by Josh Lake[36] for his master thesis titled "Development and Verification of a Test System to Quantify Strain of an Optical Displacement Indicator and the Design of a Strain Indicating Prototype".

Prototype 1

The spectral ruler concept was incorporated on to the first screw prototype to study the change in color with respect to the extension caused by loading the screw. Prototype 1 design was started by modifying a normal 2.75 inch 3/8-16 allen head screw as shown in Figure 2. 2. It consisted of four parts namely, the screw through the center of which a hole was drilled all the way from the head to the bottom. An M3x0.5 thread was tapped through this hole to accommodate the second part, an M3x0.5 threaded rod with a flat "T" shaped tip. This runs all along the center of the screw and the tip comes out of the head of the screw to connect with the spectral ruler. The transparent sheet of the spectral ruler also has a "T" shape cut out to accommodate the tip of the screw. This allows the transparent sheet to move relative to the colored sheet resulting in a gradual change in color from cyan to magenta or vice versa. The relative motion is caused by either turning the inner rod or by mechanically elongating the screw. A hexagonal prism was added on to the head of the screw in order to hold the spectral

ruler rigidly in place and the colored sheet of the spectral ruler was glued on to it to create the relative motion between the sheets. The testing for this screw mostly concentrated on the comparison between the modified screw (Prototype 1) and the unmodified screw. The cross sectional area of the prototype was 85% that of the unmodified screw and the tensile test results should that prototype 1 reached a maximum load that was 76% of the maximum load of the unmodified screw.[36] Testing with respect to the spectral ruler was hindered due to a lot of noise in the system and movement of camera and the results did not show an overall trend which was expected from the spectral ruler. The screw design had to be modified to measure clinically relevant loads and the experimental setup had to be standardized in order to reduce noise in the system. The major limitation was that the mechanism was not incorporated into the head of the screw and the color change was not reproducible.

Figure 2. 2: Assembled Prototype 1 screw[36]

Prototype 2

The design that followed prototype 1 was made from scratch from a block of steel instead of modifying an existing screw. Prototype 2 consisted of seven parts namely, the 2.5 inch 3/8 – 16 screw, M3x0.5 threaded inner rod, a wedge, a spring, a containing wall, 0-80 bolt, and the spectral ruler as shown in Figure 2. 3 (C). The working mechanism of the screw is shown in Figure 2. 3 (A). From Figure 2. 3 (B) it can be seen that the wedge has dove tails on either side which allows it to slide along the head of the screw when the screw is elongated or compressed and the spring helps in pushing the wedge back to its initial position. The wedge was made to be at an angle of 35º which gives a mechanical advantage of 1.43. The 0-80 bolt and the wall contain the wedge inside the head of the screw. The longitudinal motion or the extension in the screw is translated into transverse motion by this mechanical system. The preliminary testing of prototype 2 involved revolution testing and the results showed that the average color change per $1/8^{th}$ revolution was about 14.82% which was off the expected value by 6.7%. This was due to the fact that the revolutions were turned by hand which might not have precisely turned the inner rod $1/8^{th}$ of a revolution every time.[36]

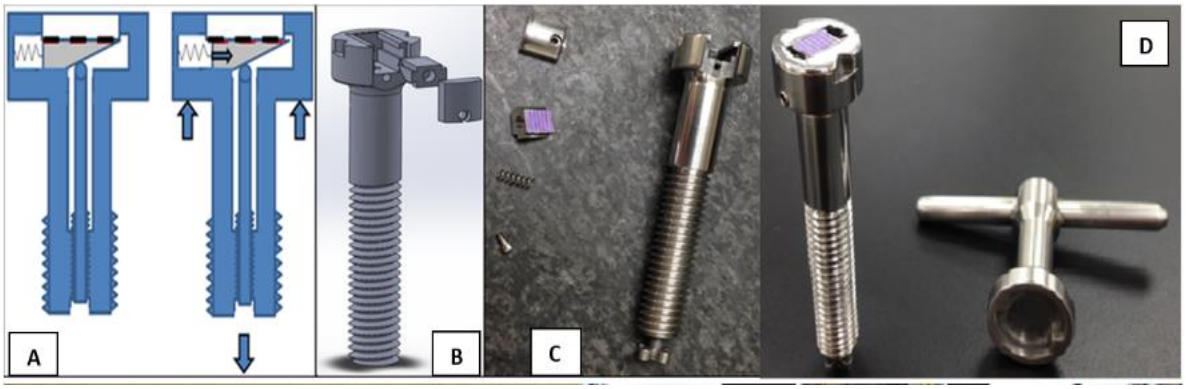

Figure 2. 3: Prototype 3 screw (A) Schematic showing working of screw, (B) SolidWorks exploded view, (C) Disassembled view with all the components, (D) Assembled view with custom screw wrench [36]

The tensile testing of prototype 2 was hindered because of an Instron malfunction resulting in the failure of the prototype 2 screw. The prototype 2 screws were then fabricated by rapid prototyping using Poly-Jet Modeling (PJM) as shown in Figure 2. 4 (A). The buildup material used was VeroClear RGD810 plastic and machine used was Stratsys Objet350 Connex. A number of these screws were tested and modifications were made to reduce the noise in the system and also continuous improvements were made to the test setup to standardize it for all tests.

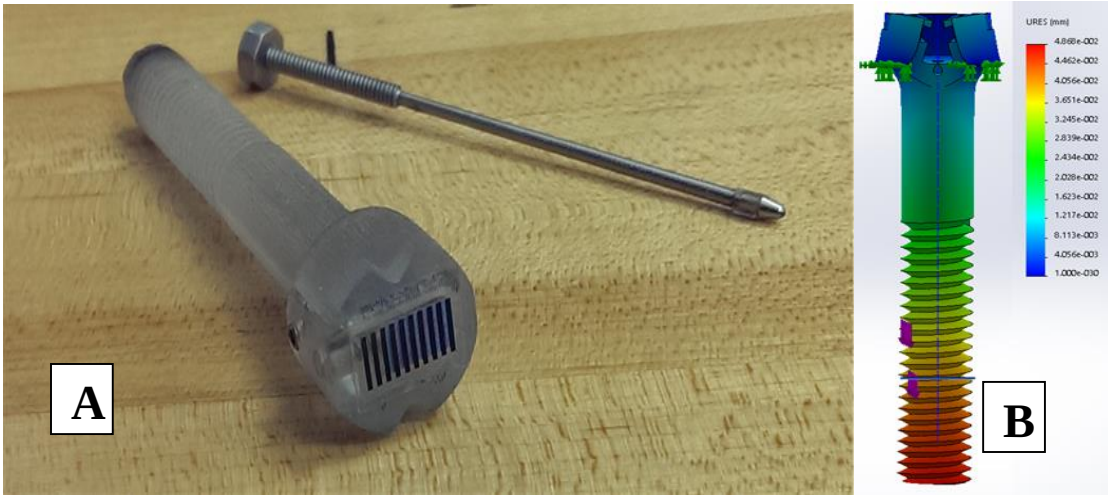

Figure 2. 4: (A) 3D printed Prototype 2 screw with inner rod (B) Simulation of SS Prototype 2 screw

The results from the cyclic tensile testing showed that screw mechanism has good repeatability and reproducibility with respect to the spectral ruler with 500 micron lines. In order to measure smaller clinically relevant strain values of 50 – 100 μm a spectral ruler with 100 micron lines had to be incorporated on to the screw for which the screw had to withstand higher loads. Also, a closer simulation analysis of the Prototype 2 design showed buckling of the screw head as shown in Figure 2. 4 (B).

Prototype 3

The prototype 3 screw design was started by modifying a normal 2.75 inch 3/8-16 allen head screw. Similar to the previous design, an M3x0.5 thread was tapped through this hole to accommodate the inner rod. Prototype 3 consisted of seven components namely: the stainless steel 316L allen head screw (70 mm long, 9.3 mm shaft dia., and 3 mm cannulation), the inner rod (2 mm diameter, 70 mm long with thread M3 x 0.5 x 9 mm), a wedge, two circular rails, two springs, the spectral ruler, and a screw cap as shown in the below Figure 2. 5. A lathe was used to turn the hex head of the screw into a circular head and Wire Electrical Discharge Machining (WEDM) was used to cut rectangular slots on the screw head to incorporate the circular rails. A 3 mm long collar was press fit near the neck of the screw to prevent the inner rod from bending.

Figure 2. 5: Prototype 3 components and assembly

The purpose of prototype 3 was to design a mechanism which would be more sensitive when compared to the prototype 2 design by reducing the resistance in the wedge sliding mechanism and also be simple enough to replicate it on an orthopaedic screw at a much smaller scale. The design from prototype 3 was miniaturized to fit into a clinically used orthopaedic screw in order to measure the repeatability and reproducibility of the screw system when subjected to clinically relevant loads. One other requirement was to be able to calibrate the screw system for measuring strain in terms of color change on the spectral ruler.

Orthopaedic Screw

The design of a strain-indicating orthopaedic screw shown in Figure 2. 6 was started by modifying a clinically used cannulated orthopaedic screw (Stainless Steel 316L) with dimensions 65 mm length, 5mm shaft dia., and 3 mm cannulation. The design of the working mechanism of the orthopaedic screw was based off of a modified 70 mm long, 9.3 mm shaft dia., and 3 mm cannulation allen head screw (Stainless Steel 316L) as shown in Figure 2. 5. It consisted of the following components: an inner rod, a wedge, two circular rails, two springs, the spectral ruler, and a screw cap. These mechanical components were miniaturized to fit into the orthopaedic screw by making few modifications. A lathe was used to turn the hex head of the screw into a circular head, Wire Electrical Discharge Machining (WEDM) was used to cut slots on the screw head to incorporate the two rods as rails, a 3 mm long collar was press fit near the neck of the screw, and a 6.5 mm long cylindrical shaft with internal thread (0.5 mm pitch) was press fit to the base of the screw. All the parts and modifications were done by Clemson University Machining and Technical Services and were manually assembled into the screw.

Figure 2. 6: Modified Orthopaedic Screw

The design of the wedge and rail system was simulated with respect to four designs as shown below. The purpose of the simulation was to check for bending of the rails and to restrict the buckling in the screw to minimum. The first design consisted of two circular rails sliding through two symmetrical holes in the wedge as shown in Figure 2. 7. The second design again had the same two rails but the wedge had two semi-circular slots on either side of the wedge instead of holes as shown in Figure 2. 8. The third design consisted of a flat rectangular rail whose width to height ratio was greater than 1 and the wedge had a rectangular hole in its center as shown in Figure 2. 9. The fourth design had two rectangular rails whose width to height ratio was less than 1 and the wedge had two symmetrical rectangular holes in it as shown Figure 2.10.

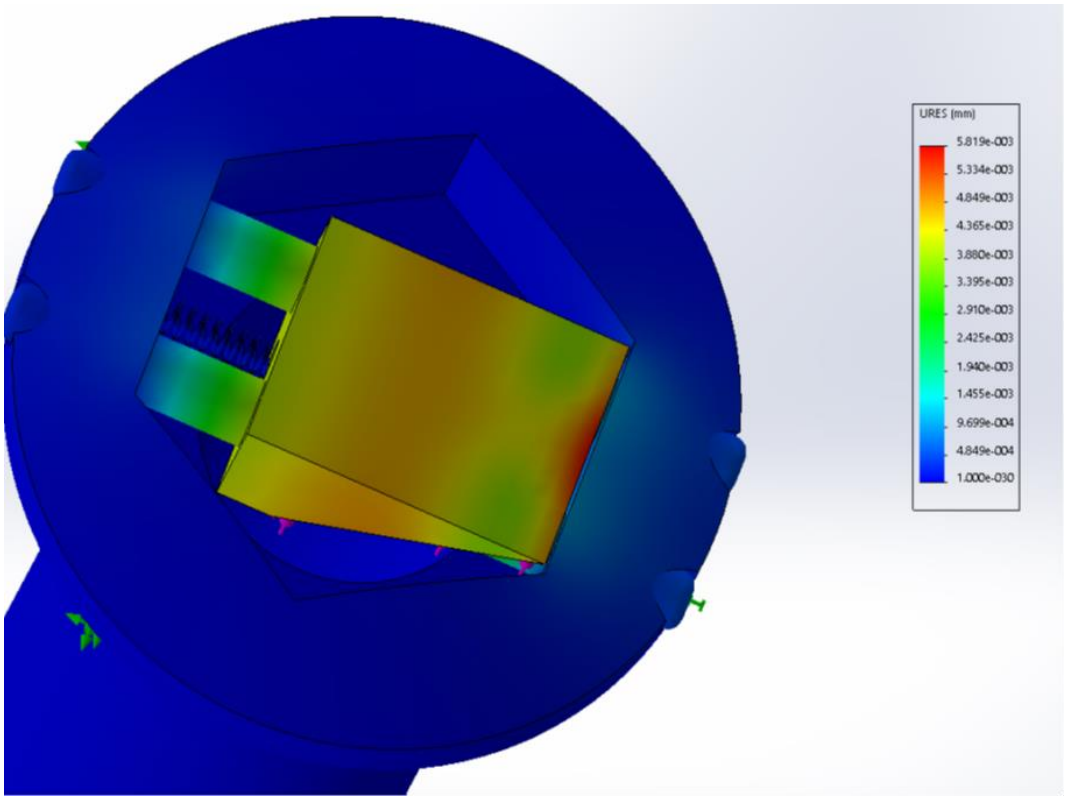

Figure 2. 7: Cannulated screw with two circular rails

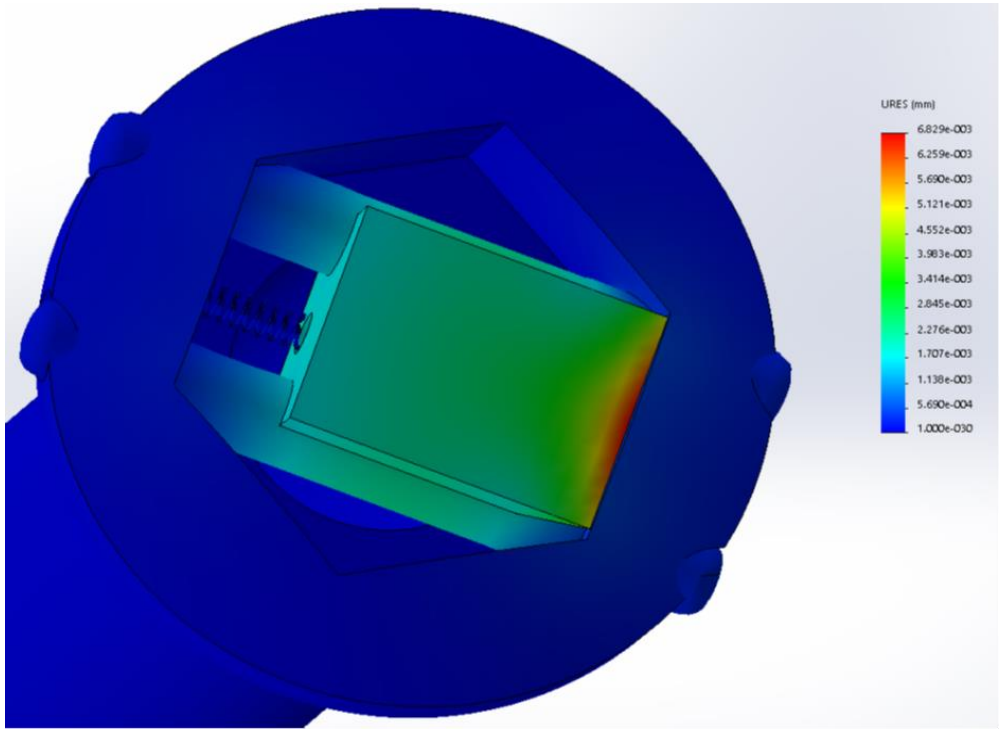

Figure 2. 8: Cannulated screw with circular rail slots

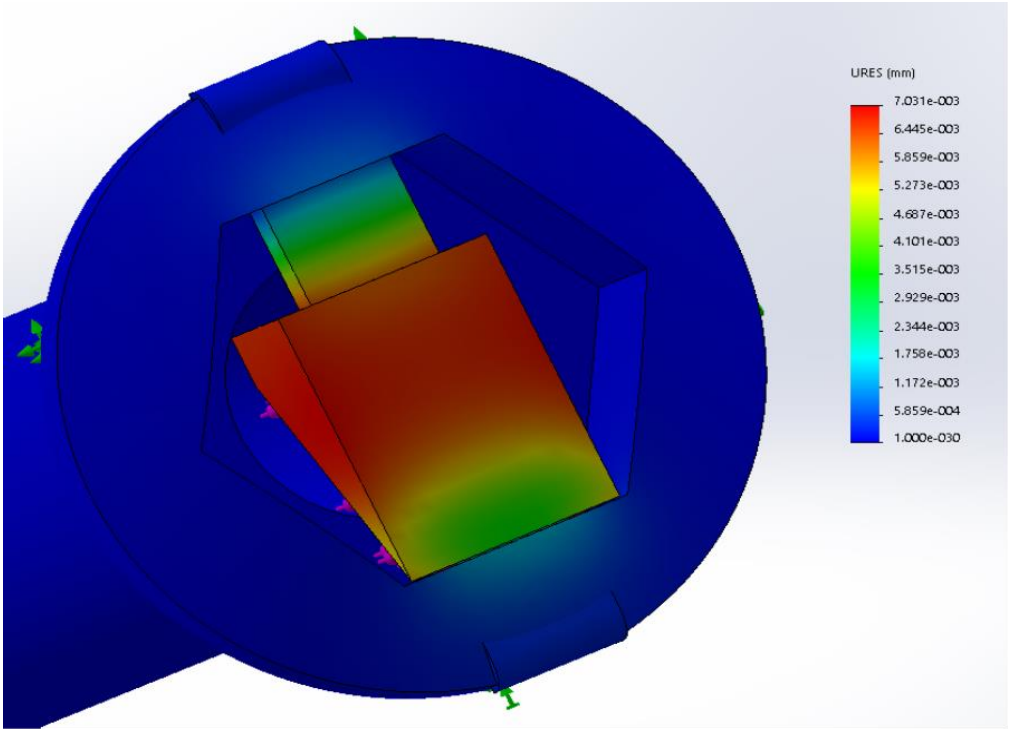

Figure 2. 9: Cannulated screw with rectangular slot

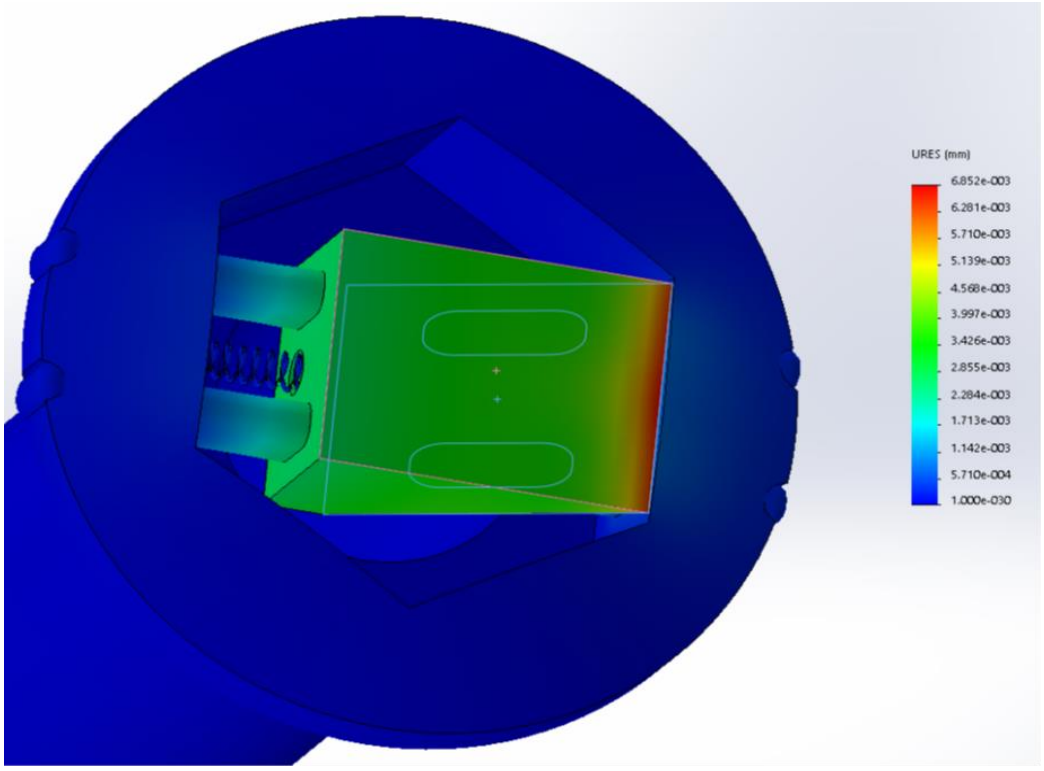

Figure 2.10: Cannulated screw with two rectangular rails

The simulation results showed that the third design with the rectangular slot was experiencing higher bending when compared to the others and was ruled out. Comparing the first two designs, the second design was able to incorporate circular rails of larger diameter when compared to the first design which would theoretically result in lower bending. But, with this design there was a possibility of the wedge tilting and the tolerance needed very higher. Finally, comparing the first and the fourth, design four showed that it deformed a little less when compared to the circular rails. The first design was selected based on the ease of fabrication and assembly. The design was further modified to include two springs around the two circular rails instead of one single spring in the center. This resulted in a uniform compression and extension of the spring and uniform movement of the wedge.

CONCEPT

The extension in the screw is a longitudinal motion and to translate this on to the spectral ruler which is a transverse motion, a mechanical system is used. The translation mechanism consists of an inner rod, a wedge running on two circular rails, and two springs centered on the rails and constrained between the wedge and the screw head. The inner rod is screwed into the orthopaedic screw and the concave tip runs along the bottom surface of the wedge (slope of 35º). Figure 2. 11 shows the movement of the wedge relative to the longitudinal extension of the inner rod (caused due to revolution of the inner rod or tensile force applied). This whole system acts as a sensor with a resolution which is controlled by the slope of the wedge and line spacing. The transparent sheet of the spectral ruler is fixed to the screw head cap whereas the colored sheet is fixed on to the top surface of the wedge. Relative horizontal motion between the two sheets produces a change in color visible through the transparent spaces.

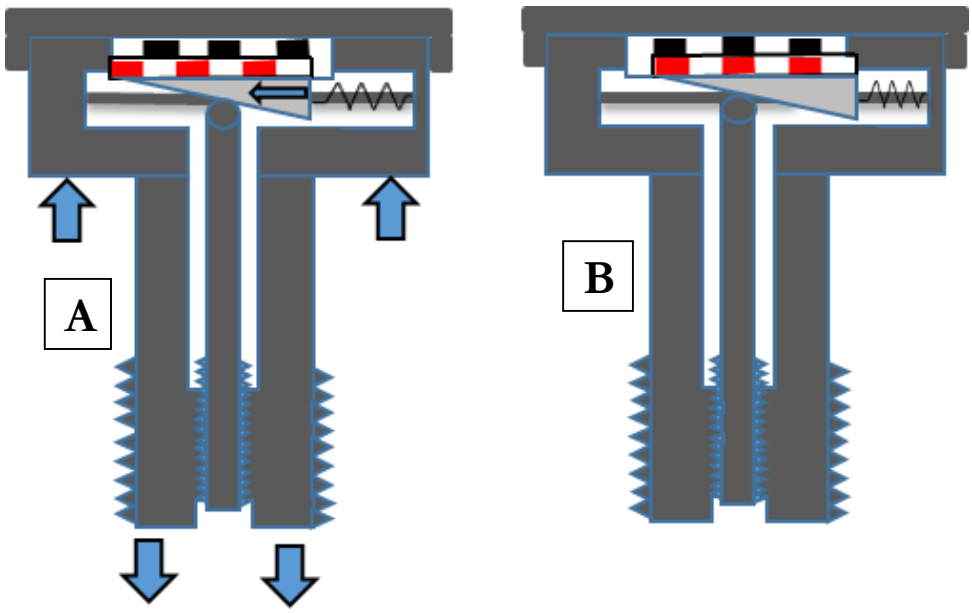

Figure 2. 11: Concept A) Screw under tension, B) Screw without tension

CHAPTER 3

VALIDATION OF ORTHOPAEDIC SCREW PROTOTYPE

METHODS

The testing was carried out in the Laboratory of Orthopaedic Design and Engineering at Clemson University, where the ambient temperature was noted to be 66ºF and 40% relative humidity. The lab windows around the testing area were shielded to block the sunlight. This was done to maintain constant lighting irrespective of the time of the day the testing was carried out.

Experimental Setup

An Instron 8874 Axial-Torsion Fatigue Testing System was used to carry out all the testing on the orthopaedic screw and the experimental setup is as shown in Figure 3. 1. It is a bi-axial tabletop servohydraulic testing system providing a combined axial and torsion dynamic actuator in the upper crosshead which has an axial force capacity of up to ±25 kN (5620 lbf) and torque capacity of ±100 Nm (880 in-lb). An Epsilon 3542 Extensometer (accuracy: ± 1 μm) with a gauge length of 2.00 in. and travel of ± 0.200 in. (±10%) was used throughout the test to measure the extension between the head of the screw and the hydraulic grip holding the screw.

The test setup consisted of the test specimen, extensometer, hydraulic grip, U-shaped fixture, two sliding fixtures, camera, light source, and mirror. The hydraulic grip shown in Figure 3. 3 was custom designed to hold orthopaedic screws of different lengths and the length of the screw being gripped can also be varied. The U-shaped fixture was designed to hold the

head of the screw to create tension in the screw when the load was applied by the Instron. Since the screw had to be placed inverted, a mirror was used to reflect the image on to a camera. In order to maintain consistency between tests a few custom fixtures were designed and fabricated. The requirement was for a fixture that can provide stability and maintain the position of three independent components namely, a camera, a light source and a mirror with an option to be able to change the position of the three devices relative to each other. A set of sliding fixtures as shown in the Figure 3. 2 were machined and assembled together to hold the camera and light source in the same place to obtain repeatability in all tests. The camera and light source fixtures slide opposite to each other and are adjustable according to the need of the experiment, they can move front and back and the height is adjustable with the help of long threaded rods and a pair of nuts.

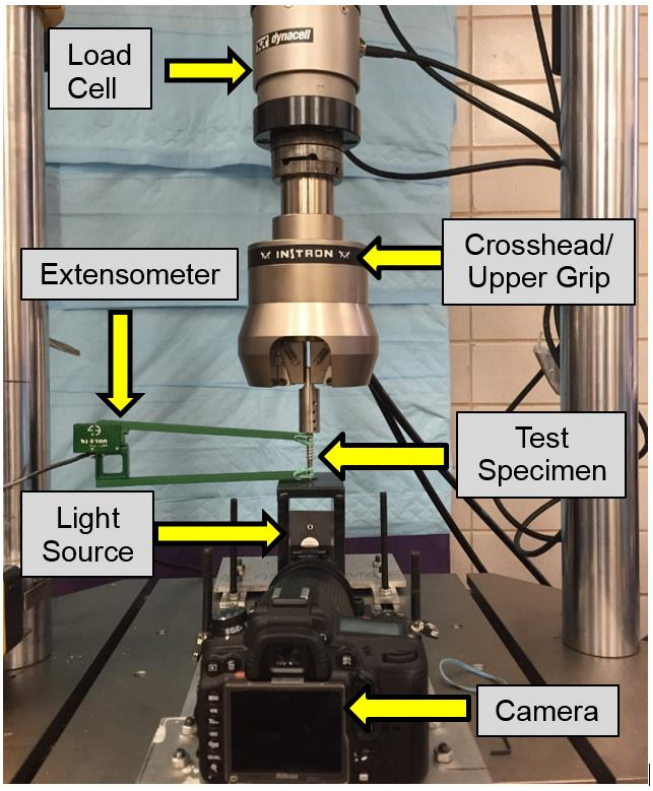

Figure 3. 1: Experimental Setup

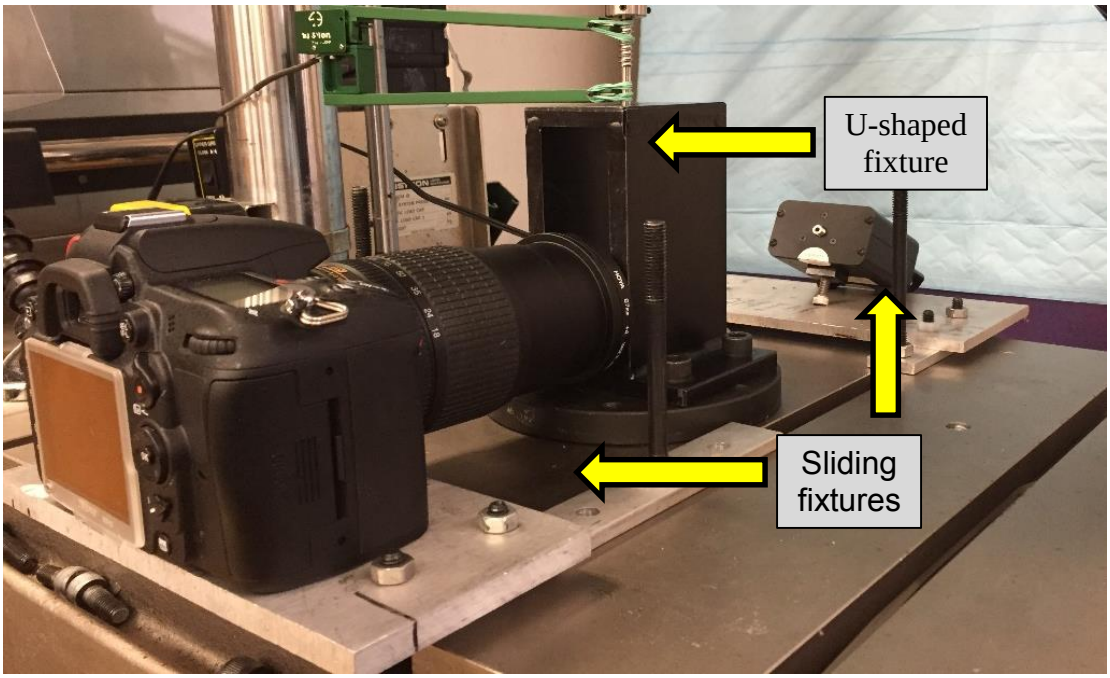

Figure 3. 2: Fixtures for setup

Figure 3. 3: Hydraulic grip

Test methodology

Bluehill 2.0 testing software and WaveMatrix Dynamic testing software of Instron were used for all the testing. The inner rod was screwed into the test specimen i.e., the orthopaedic screw to check for contact with the wedge. The initial position of the wedge was when only the white color was visible through the spectral ruler. The screw was then held by the U-shaped fixture with the help of washers to make sure the tensile force was distributed uniformly over the head of the screw. The hydraulic grip was used to safely and securely hold the test specimen in the Instron during testing. Before every test the orthopaedic screw was auto tuned at 50% of the maximum load applied during testing. All the tests on the orthopaedic screw were load controlled and cyclic. The first test was a cyclically loaded test for 5 cycles of a triangular waveform. The ramping rate for loading was 10 N/sec with no hold and images were captured by the camera every 2 seconds. The second test was a cyclically loaded test for 5 cycles of a trapezoidal waveform with a preload of 500 N and a maximum load of 2000 N for the first cycle which decreased by 250 N every cycle. The ramping rate for loading was 1/100 N/sec of the maximum load of each cycle, the hold was for 60 seconds each cycle, and images were captured by the camera every 2 seconds. The third test was a higher frequency cyclic loading for 50 cycles of a triangular waveform. In this test the orthopaedic screw was preloaded to a 1500 N and a 500 N load was fluctuated every sec above and below the preload value. Each cycle lasted for 4 seconds and the images were captured every second. The test methodology is summarized in the Table 3.1 below.

	Parameters						
Test No.	**Waveform**	**Spectral Ruler (μm)**	**Preload (N)**	**Load Range (N)**	**Loading Rate (N/s)**	**Hold Time (s)**	**Image Capture Time Interval (s)**
1	5 cycle Positive Triangular	100	500	2000	7.5	0	2
2	5 cycle Positive Trapezoidal	100	500	Cycle 1: 500 - 2000 Cycle 2: 500 - 1750 Cycle 3: 500 - 1500 Cycle 4: 500 - 1250 Cycle 5: 500 - 1000	7.5 6.25 5 3.75 2.5	120	2
3	50 cycle Triangular	100	1500	2000	500	0	1

Table 3. 1: Test Protocol

Data acquisition and analysis

The test data was acquired by the Instron at a frequency of 10Hz and it consisted of the total time (seconds), total number of cycles, load (N), displacement (mm) of the Instron actuator arm, and the extension (mm) from the extensometer. The required data points were filtered out depending on the rate of images captured for different tests. A Nikon D7000 digital camera was used to capture videos and images at various intervals depending on the type of test. The camera was controlled through 'Camera Control Pro 2' software installed on a computer. Images were captured with an aperture of f/5.6, exposure time of 1/6 second, and focal length of 105 mm with manual focus. A +4 lens was added to the camera in order to move the camera closer to the specimen and achieve a better focus. A Tungsten Halogen light source was used to make sure the light was constant in every image captured throughout

the test. The images were analyzed using MATLAB software to quantify the amount of color change and the code is as seen in Appendix (A).

The picture number and XY pixel range is input into the code which then outputs the mean amount of red, green and blue in each photo and from the mean values, R', G' and B' are calculated using Equation 3.1 below.

$$G' = \frac{Green_{mean} - Green_{minimum}}{Green_{maximum} - Green_{minimum}} \quad (3.1)$$

After R', B' and G' are calculated for each image, a ratio is determined for each photo using Equation 3.2 below:

$$Green : Blue\ Ratio = \frac{G'}{(G' + B')} \quad (3.2)$$

This ratio is then graphed versus the corresponding photo number in order to see how the optical displacement indicator changed color ratios throughout the test. The ratios range from 0 to 1 with 0 corresponding to the least amount of green and 1 corresponding to the most amount of green.

RESULTS

The processed image data from MATLAB and Instron data were consolidated and the results obtained from each test were plotted on graphs as shown below.

Test 1

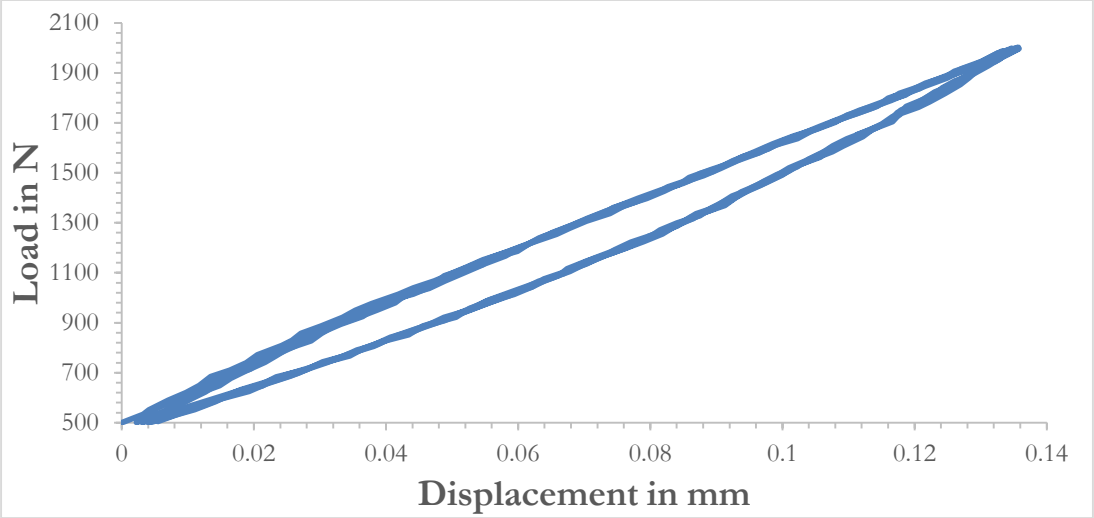

Figure 3. 4: Test1 – Load v/s Displacement (Hysteresis)

The Figure 3. 4 shows the load vs displacement graph and the area under the curve gives the hysteresis, or the work done by the orthopaedic screw due to loading and unloading over 5 cycles. The amount of work done was consistent and approximately equal to 0.323 Joules. The graph in Figure 3. 5 shows the color change in the spectral ruler due to the tensile load applied on the orthopaedic screw. The color change seen for an applied load of 1500 N was about 0.83 on a scale of 0 to 1. Figure 3. 6 shows the color ratio vs load graph and the area under the curve gives the hysteresis due to the wedge system of the orthopaedic screw over 5 cycles. The loss in the amount of energy was consistent and approximately equal to 1296 N*color ratio (scale 0-1).

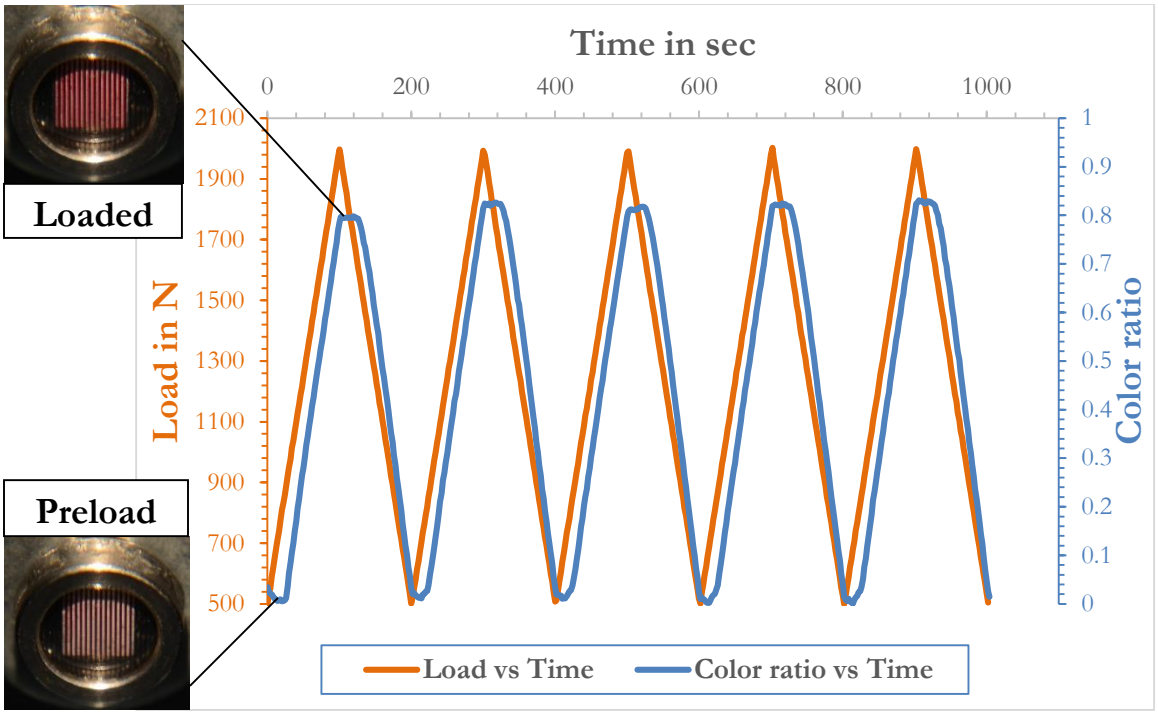

Figure 3. 5: Test1 - Color change(in 2sec interval photos) with respect to load(± 1500 N)

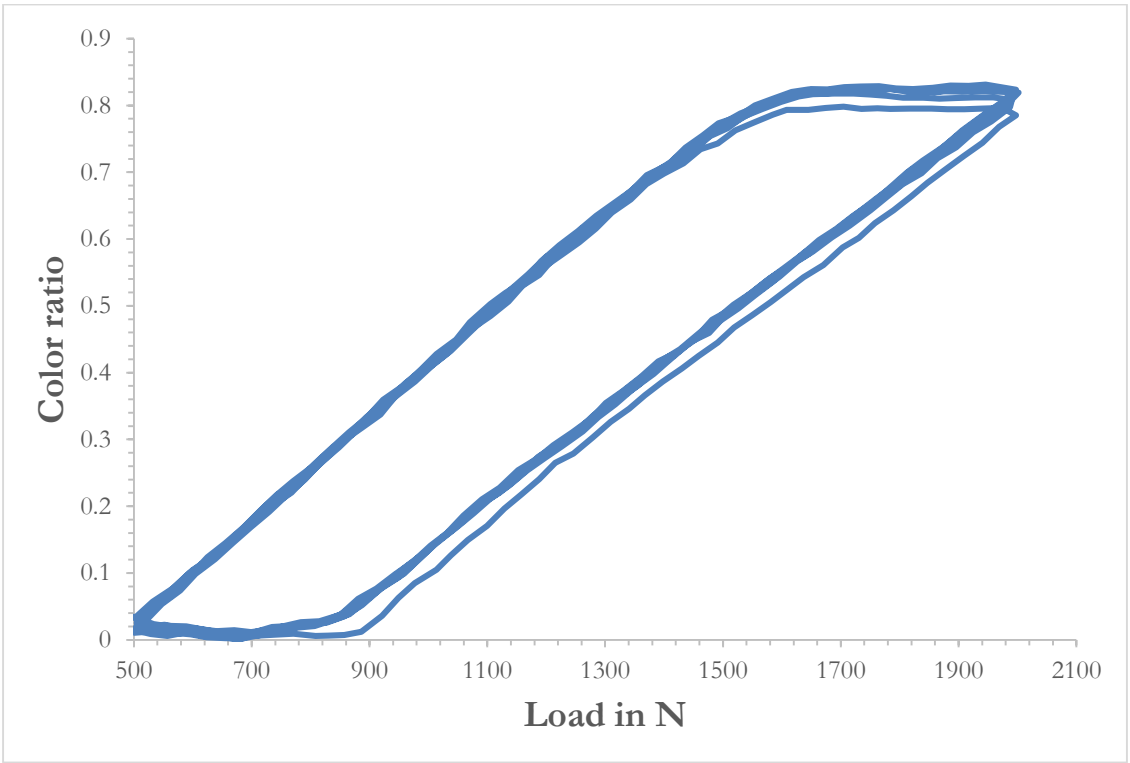

Figure 3. 6: Test 1 – Color ratio v/s Load (Hysteresis)

Test 2

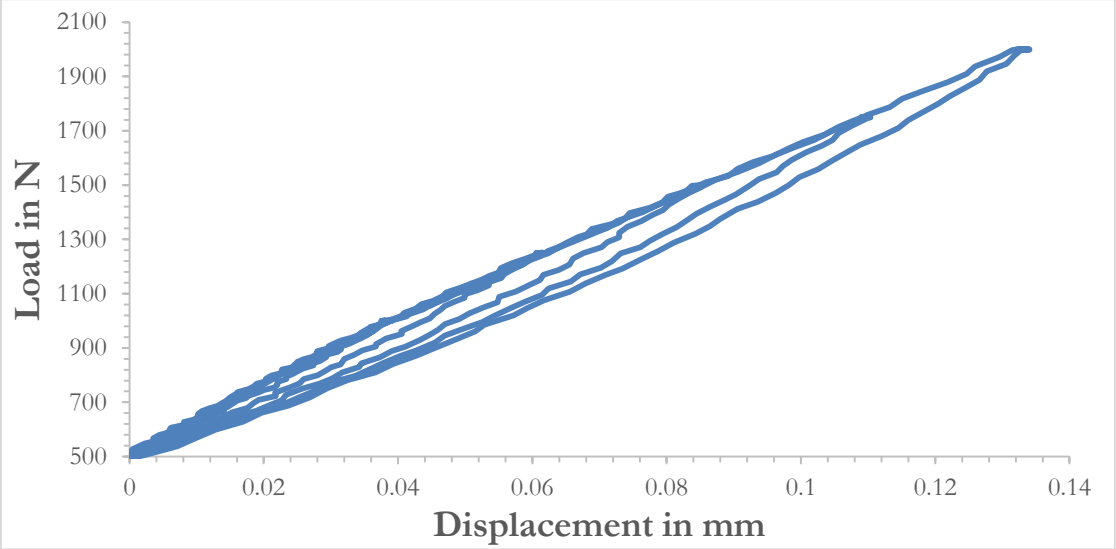

Figure 3. 7: Test 2 - Load v/s Displacement (Hysteresis)

The Figure 3. 7 shows the load vs displacement graph and the area under the curve gives the hysteresis over 5 cycles. The work done over the 5 cycle was a linear curve with maximum of 0.36 Joules and a slope of 0.95. The graph in Figure 3. 8 shows the color change in the spectral ruler due to the tensile load applied on the orthopaedic screw. The color change seen for applied loads of 1500, 1250, 1000, 750 and 500 N was about 0.81, 0.66, 0.49, 0.31 and 0.12 respectively on a scale of 0 to 1. Figure 3. 9 shows the color ratio vs load graph and the area under the curve gives the hysteresis due to the mechanism of the wedge system of the orthopaedic screw over 5 cycles. The loss in the amount of energy was a liner curve with a maximum of 1332.56 N*color ratio and a slope of 0.98. Assuming that the load from the Instron is constant, the noise or resolution in the system was calculated at hold positions of each cycle and the average was found to be equal to 0.00119 color change corresponding to 2.17 N.

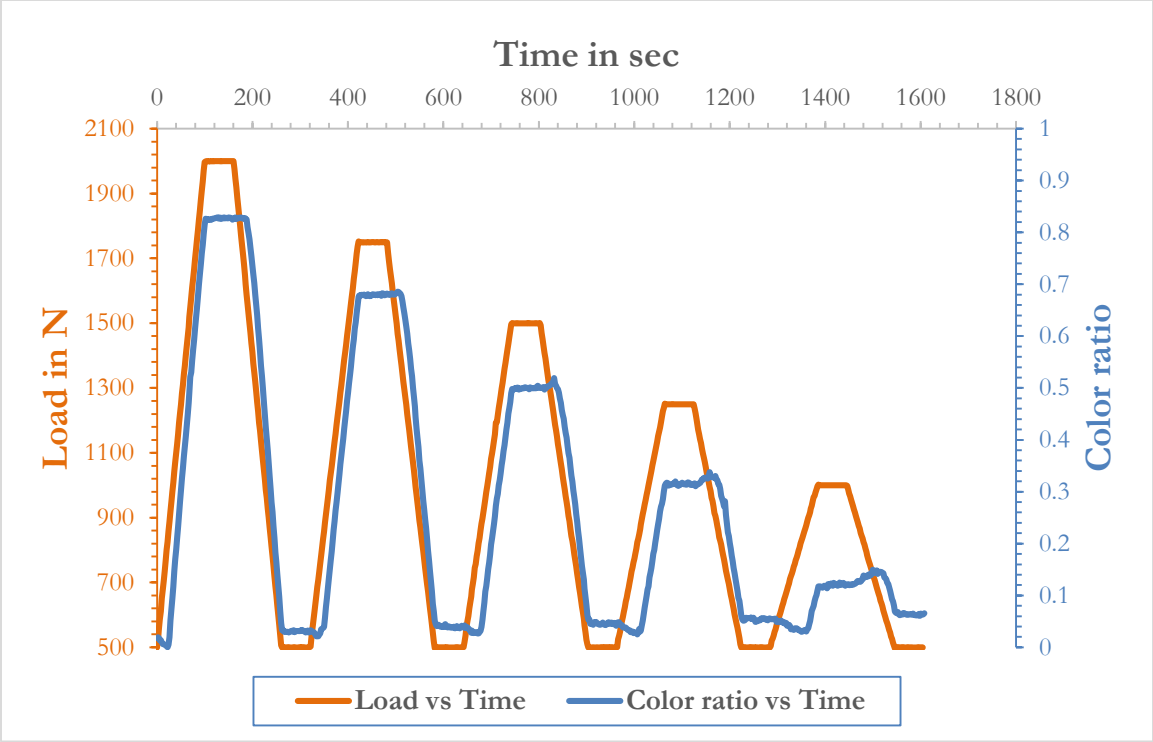

Figure 3. 8: Test 2 - Color change (in 2sec interval photos) with respect to various loads applied

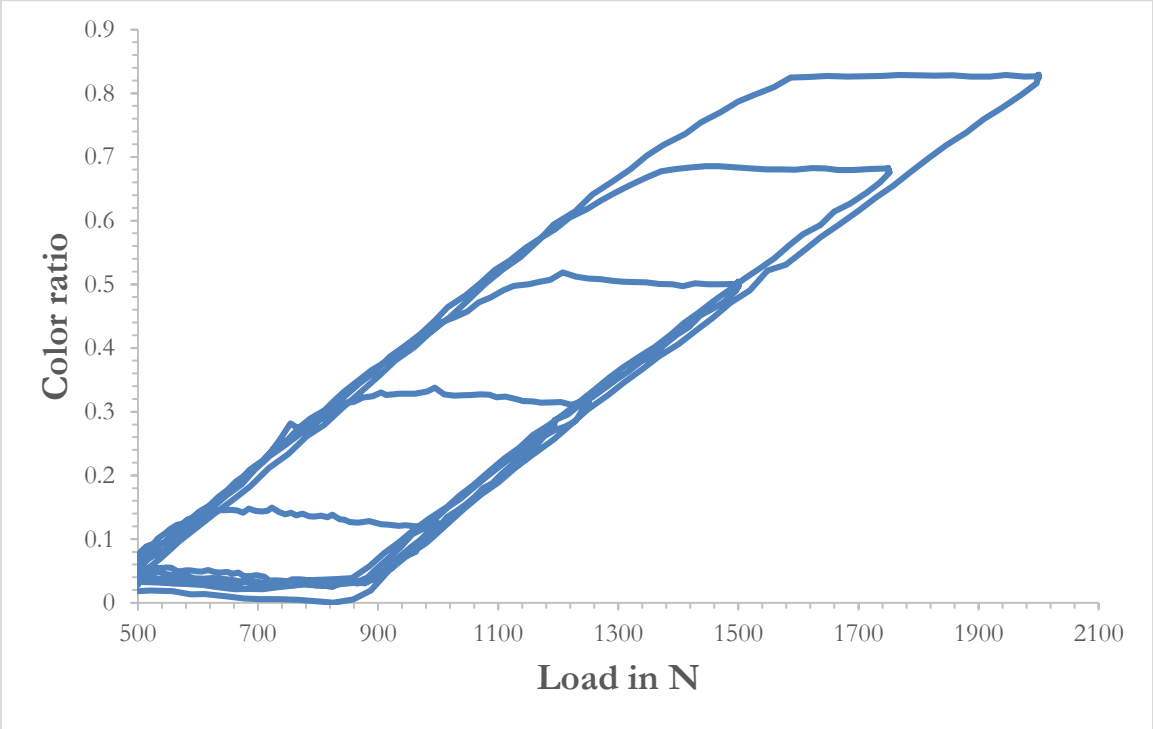

Figure 3. 9: Test 2 – Color ratio v/s Load (Hysteresis)

Test 3

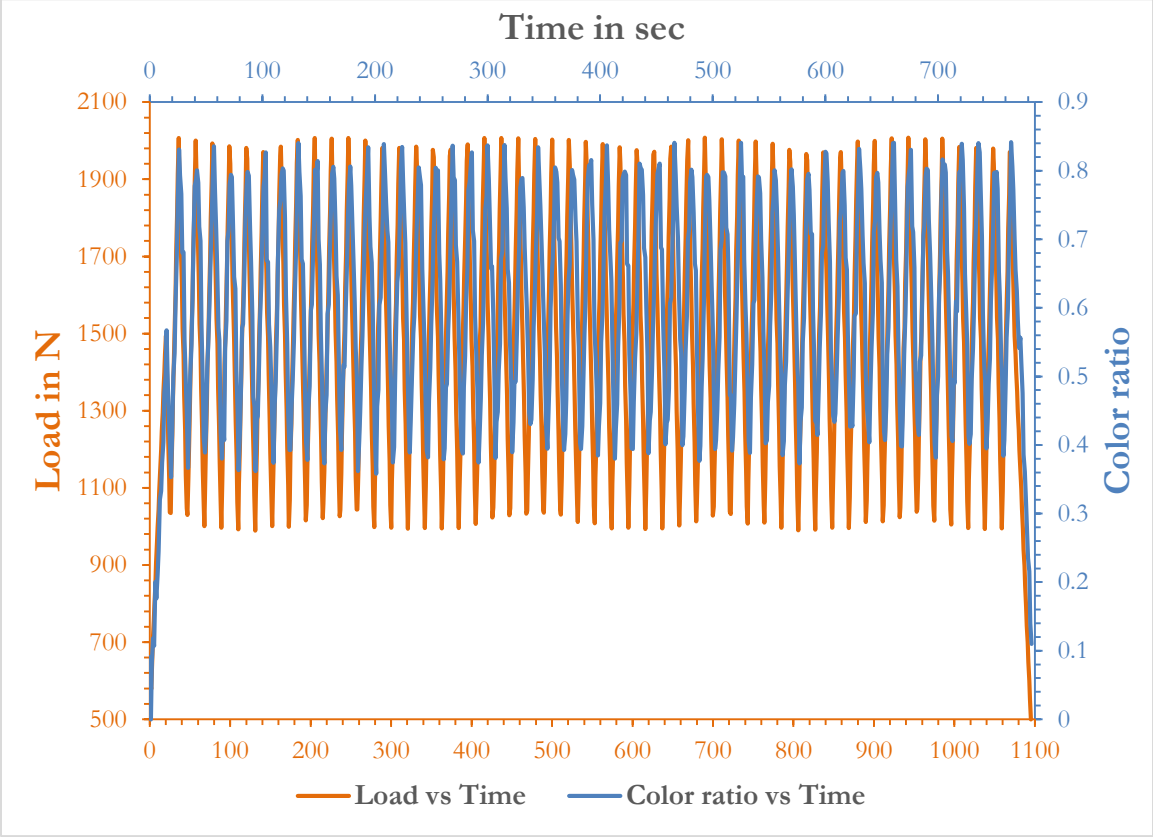

Figure 3. 10: Test 3 - Color change (in 1sec interval photos) with respect to load(±500 N)

The graph in Figure 3. 10 shows the color change in the spectral ruler due to the tensile load applied on the orthopaedic screw. The color change followed an increasing and decreasing trend similar to the load applied over the 50 cycles but due to lag in the images captured by the camera the load data and image data was not synced properly. The color change seen for an applied load of 1500 N was about 0.84 on a scale of 0 to 1.

DISCUSSION

The purpose of test 1 was to verify the reproducibility and repeatability of the screw to work as a tool to be able to quantify the loads applied. From the results we could see that the orthopaedic screw system with the spectral ruler had some amount of hysteresis but it was consistent for all five cycles. Similarly, the results from test 2 showed the presence of hysteresis which reduced linearly with decrease in load range value. This hysteresis is due to the material as well as the mechanical system. The hysteresis due to the mechanism alone could be due to a number of factors. Firstly the translation mechanism has a number of parts which might individually contribute to the total hysteresis like the tolerance between the holes in the wedge and the circular rails. This tolerance will determine the amount of friction it might produce during sliding of the wedge. This can be one of the main factors that also affects the response rate of the system. Secondly, the bending of the inner rod might result in a lag between the elongation in the screw and the wedge movement. This was minimized by press fitting a collar that will guide the inner rod. The contact point between the wedge and the inner rod is very crucial and the curvature of the tip of the inner screw will determine the sensitivity of the screw. The tolerance between the wedge holes and the rails can again determine the longitudinal movement of the wedge which should be as minimum as possible to prevent the wedge from sticking. Finally, spring relaxation might also result in a delayed response of the wedge during screw extension.

Since the screw should be able to detect sudden load changes caused due to infection or implant failure in the body, the hysteresis in terms of load will determine the minimum load it requires to cause a change in color after being held at a constant load. From Figure 3. 8 this

value at a constant preload of 500 N was approximately 350 N and for 2000 N and corresponding lower load in each cycle was calculated to be approximately 350 N. This is the minimum amount of load the screw needs in order to engage and disengage the sliding mechanism. Future designs will look into reducing this load threshold by reducing the hysteresis in the mechanism. For better understanding of the hysteresis in the system, the screw mechanics was analyzed in depth and can be found in Appendix (B).

Noise in the system is also a crucial part of any experiment and by reducing the noise, the efficiency of the system can be improved. So, in order to determine the noise in the system, the hold region in Test 2 was looked at more closely. Here the screw is being held at a constant load and therefore should not result in any color change theoretically. But there is always some amount of noise in the Instron and thus the load applied is not constant. Assuming the load from Instron to be constant, the fluctuations in the color was calculated and found to be 0.0012 which is equivalent to 2.17 N fluctuation in load which is the resolution of the screw. Some of the tests were conducted with black screen around the whole setup to check if the surrounding light produced any noise in the results. The results did not show any significant difference and this is also due to the fact that a constant light source was used.

The orthopaedic screw developed should have the ability to display the load value in terms of color changes and this was calculated from test 2. Due to the extensometer not behaving linearly during testing, the expected extension of the screw corresponding to the maximum load of 1500 N was obtained from Solidworks simulation as shown in Figure 3. 11 and was found to be 48 microns. This was divided by Tan 35º which is the angle of the wedge as shown in Figure 3. 12 to determine the distance by which the wedge has moved. The

distance was found to be 68.64 microns which is equivalent to 68.64% color change of a 100 micron spectral ruler. Since the color change is a ratio between 0 and 1, the absolute color change was actually found to be 56.72% which also agrees with test 1 and 3. Also, from simulation and test 2 the actually color changes with respect to the decreasing loads 1250, 1000, 750 and 500N were 38.87%, 22.83%, 10.80% and 2.74% respectively.

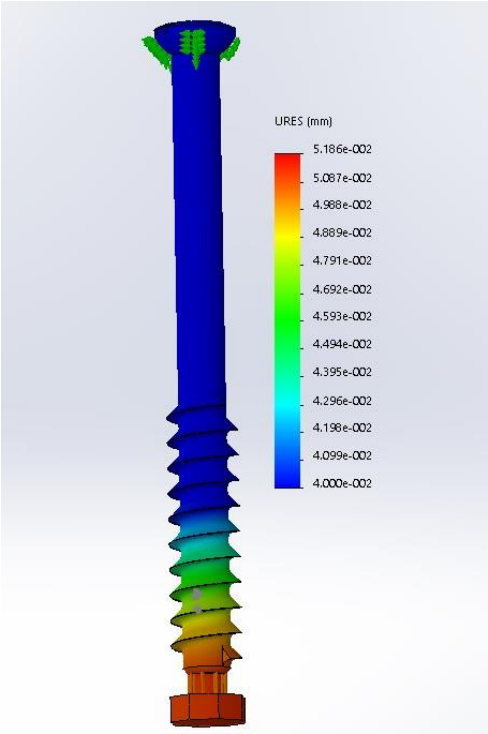

Figure 3. 11: Orthopaedic screw simulation on Solidworks

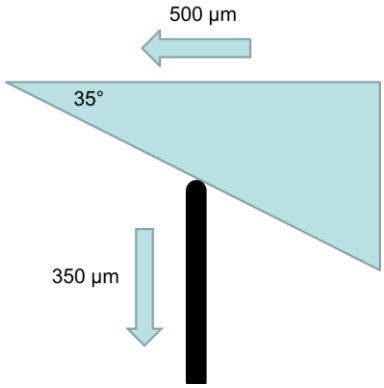

Figure 3. 12: Relation between extension and wedge movement

The idea of non-invasively tracking the load on the orthopaedic screw in vivo would not be possible without the incorporation of luminescent spectral rulers. Studies carried out by Melissa Rogalski at Dr. Jeffrey Anker's lab in the Chemistry Department involved the testing of luminescent spectral rulers with and without tissue. They consisted of two layers: a 950 micron linewidth CdSeS/ZnS core shell quantum dot interdigitated sensor were prepared with alternating QPP 645 and QPP 665 quantum dots (Ocean NanoTech) acting as the encoder and a sensor analyzer mask, printed on 3M CG 6000 multi-purpose transparency using a laserjet printer (HP color CP1518ni). The spectral ruler sample was displaced 2.0 mm back and forth by a motorized stage. The sensor was excited with a 633 nm laser during testing and sample emission was collected with a spectrometer (DNS 300, DeltaNu). The fluorescence intensity ratio 660/715 nm was calculated for each spectrum and plotted versus stage displacement as shown in Figure 3. 13, 3 .14, 3. 15 and 3. 16. For measurements through tissue, the spectral ruler was sandwiched between two pieces of 6 mm chicken breast.

The fluorescence spectroscopy results showed that the spectral ruler was able to track the displacement of the motorized stage with and without tissue. The magnitude of the ratios was much larger for the trial with no tissue and hence it was plotted on a log scale. The reason that the ratios are not the same through tissue and without tissue however is due to the autofluorescence from the tissue when excited with 633 nm light. From the below graphs it can be seen that the displacement can be measured in terms of change in spectral ratio for a tissue thickness of 6mm which is in the range of the tissue thickness around the tibia.

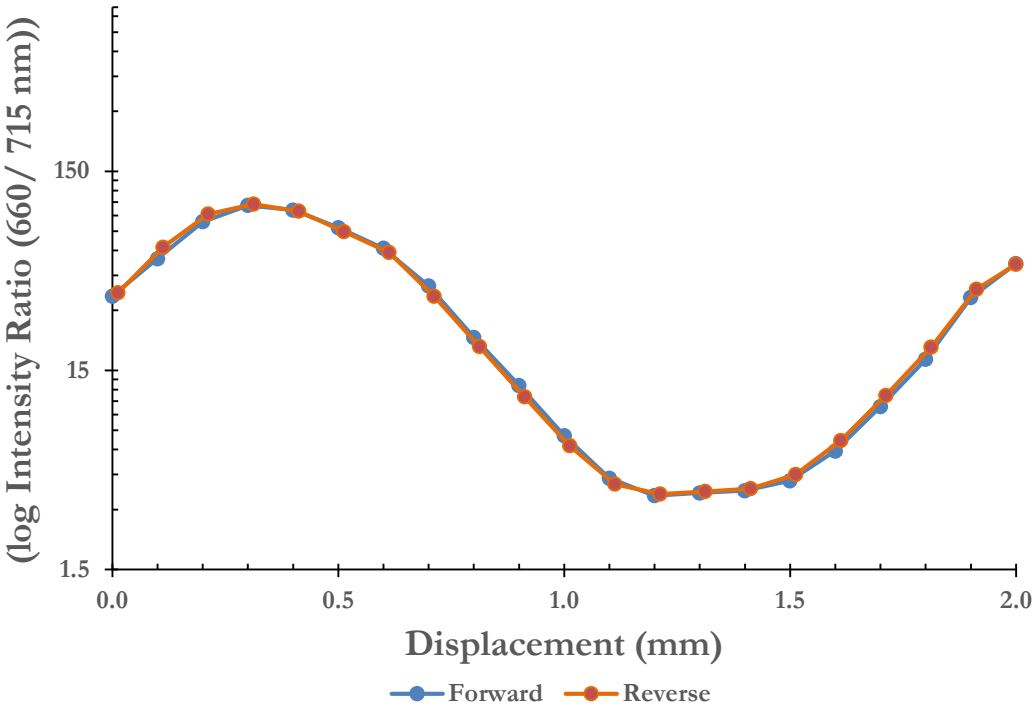

Figure 3. 13: Fluorescence intensity vs Displacement without tissue

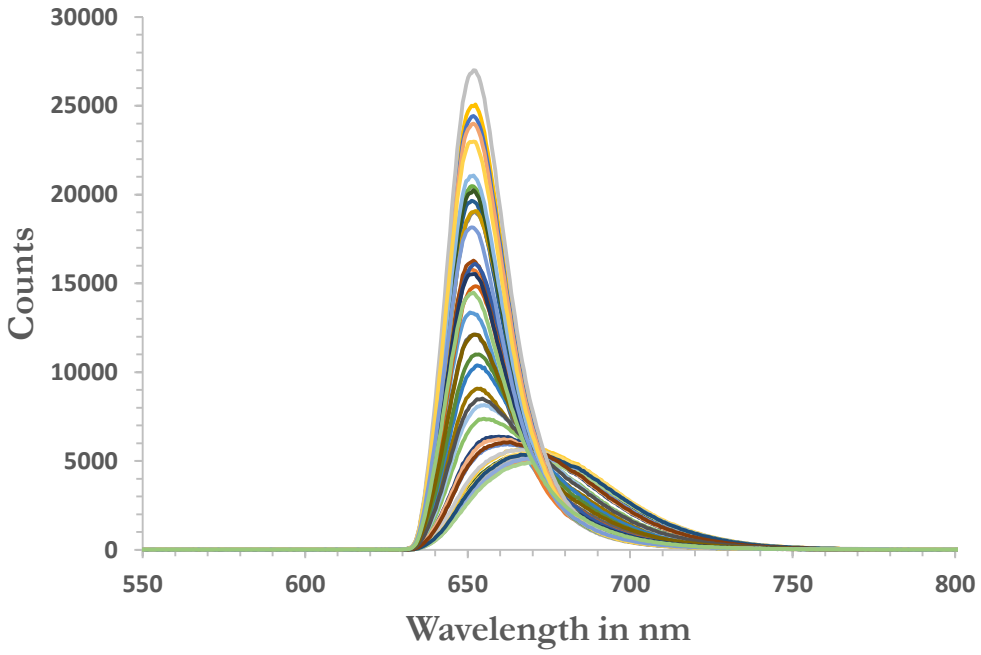

Figure 3. 14: Fluorescence spectra at 660/715 nm without tissue

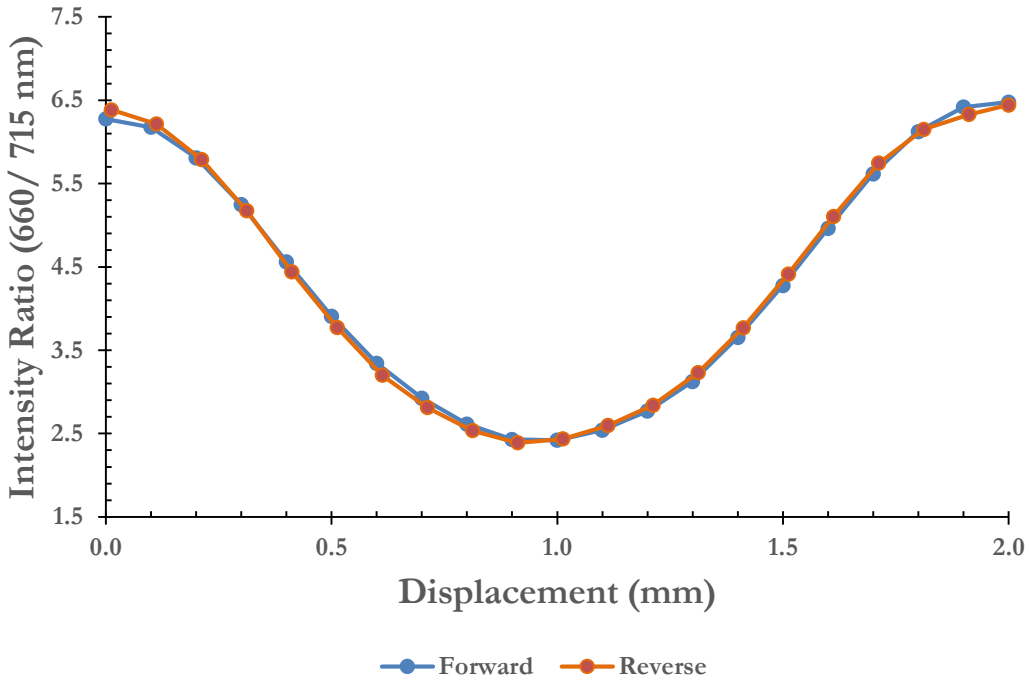

Figure 3. 15: Fluorescence intensity vs Displacement with 6 mm chicken breast

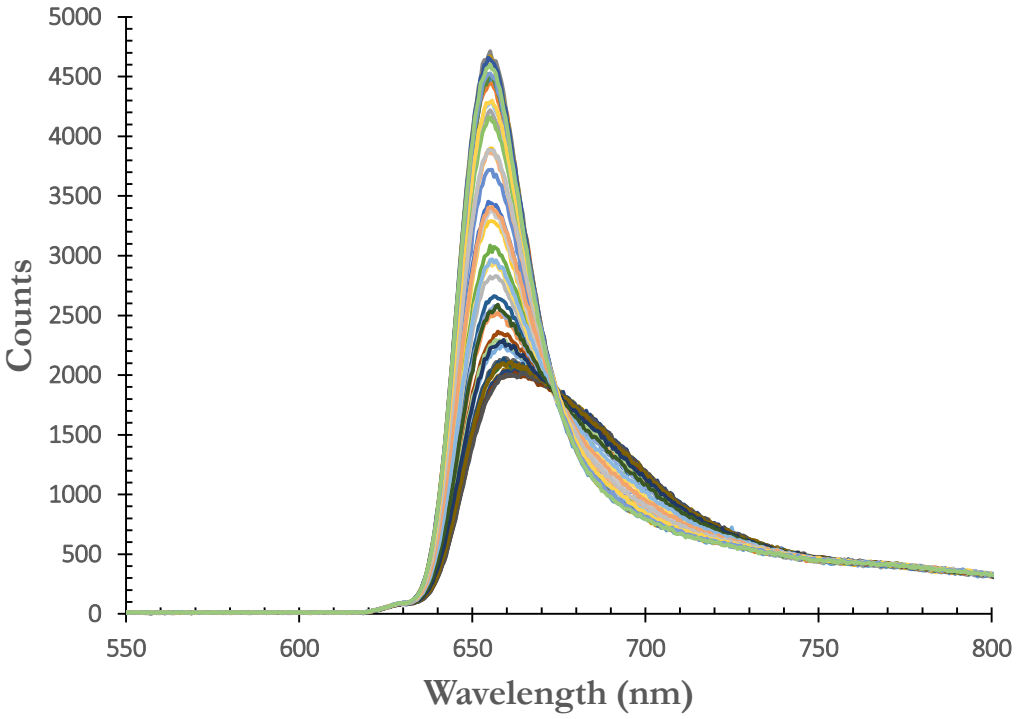

Figure 3. 16: Fluorescence spectra at 660/715 nm through tissue

CHAPTER 4

CONCLUSIONS AND FUTURE WORK

In conclusion, the research work on the orthopaedic screw provided the following outcomes: 1) The orthopaedic screw has good reproducibility and repeatability at clinically relevant loads which are vital characteristics for it to function as a tool to quantify strain on implants in vivo. 2) The load applied on the screw was quantified in terms of color ratio; a 1500 N load resulted in 68.64% color change of a 100 micron spectral ruler. The corresponding change in color can be calculated for any load valve within the load range of the screw. 3) The amount of noise or the resolution of the screw system is 0.00119 color change corresponding to 2.17 N. This was the average smallest value of color change the screw can detect with the 100 micron spectral ruler, assuming that the noise in load applied by the Instron is negligible. 4) The load threshold at loading and unloading above which the screw system gets engaged and disengaged is approximately 350N. Any load applied below this value will not produce a significant color change in the spectral ruler.

Throughout the series of tests conducted from one prototype to another, a variety of system changes were implemented in order to decrease noise from the spectral ruler data and increase accuracy of the strain indicating test system. Optimal image focus, consistent light intensity and consistency in the experimental setup were crucial in obtaining the repeatability and reproducibility of the screw system. The addition of fixtures to stabilize various components of the test system significantly improved the setup time and also the efficiency of the system as a whole. The use of Tungsten Halogen lamp behind the specimen also assisted in not only better focus, but also increased consistency of light intensity in each photo. Future

tests need to continue to increase the sampling rate, taking multiple pictures per second. Also, the synchronization of the photos with the Instron can be achieved by making use of a trigger system on the Instron. The biggest difficulty faced was in aligning the 100 micron spectral ruler layers perfectly parallel and on to the head of the screw. This issue was solved by incorporating a cap which could be rotated to align the spectral rulers and then fixed in the required orientation. Once the attachment method of the spectral ruler was improved and the system improvements described above were applied, the photo analysis of the spectral ruler data proved to be accurate and follow the same trend of the Instron.

The work presented in this research also gives a brief background on the evolution of screw prototypes leading to the development of the orthopaedic screw. This helps to understand the need for design changes that took place during the transition between prototypes. Next generation designs can study the evolution for drawbacks and develop more efficicent systems. The orthopaedic screw system developed was able to quantify clinically-relevant bone healing strains and also exhibited good repeatability and reproducibility. However, it did possess some amount of hysteresis due to the mechanism of the screw which will be reduced in the next generation designs. The findings in this research show encouraging results which will help develop a unique portable tool for physicians to quantify bone healing, implant loosening and/or infection in vivo rather than relying on less quantitative assessments based on pain and radiography.

Future work will look more closely into bending in screws which is also a common phenomenon in orthopaedic screws, especially when implanted in combination with plates. A next generation prototype for the orthopaedic screw is being developed to reduce the

hysteresis in the system and also be capable of providing a mechanical advantage of 10 through the pivot-hinge mechanism as shown in Figure 4. 1. Future work will also involve the incorporation of luminescent spectral rulers in orthopaedic screws and tested on cadaver models.

With this approach we can provide a very simple, sensitive, non-invasive, and highly versatile strain gauge based on optical fringes which can be easily fabricated with biocompatible materials. This system can be easily applied onto dynamic compression fixation plates and implant screws or bolts. It can also be easily modified to investigate many different biomechanical problems including bone healing with intramedullary nails, endodontic osteointegration, tendon repair, intrafragmentary gauges, and muscle atrophy.

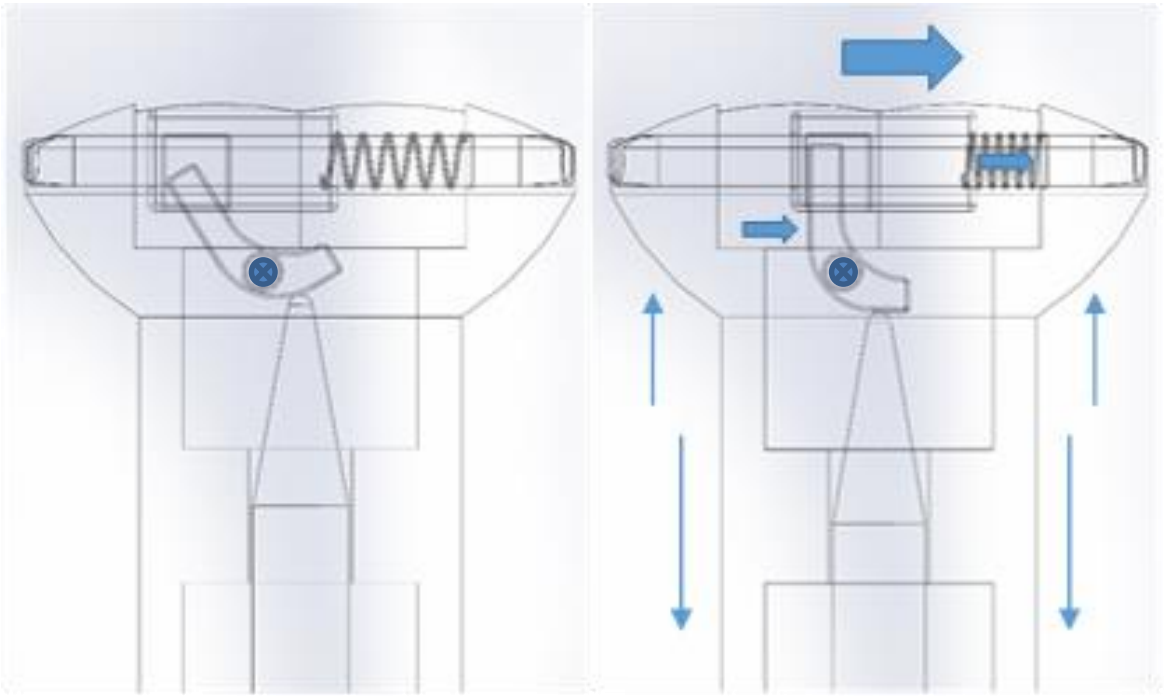

Figure 4. 1: Pivot-hinge design for orthopaedic screw

The screw transaltional mechanisms in each prototype discussed above have resulted in hyteresis due to the combination of different mechanical components. Thus reduction in the number of components would result in a more efficient system. One such concept would be a screw design with an elastic band to replace the wedge. The elastic band expanding or contracting under tension or compression would not only increase the senstitivity of the tool but also would be easy to fabricate and minituraize to the required size. Beyond the concept of a strain indicating system for orthopedic plates and screws, there are many other applications the concept can be applied to. The screws can be coated with biocompatible luminescence materials so as to indicate the change in strain on the surface of screws or plates which would give a much detailed and real time tracking of the strain on implants. This can be extended to any material and thus be able to monitor the healing of injured tendons, ligaments and muscles.

APPENDICES

APPENDIX A

Photo Analysis MATLAB Program

```
function[III,I, R, G,
B,Rm,Gm,Bm]=imageanalloada8(S,x_range,y_range)
 filename= input('Enter the filename','s');

% This function loads all files in a specified directory,
sequentially by time,
cd(uigetdir);
Fst=dir;
Fst=Fst(3:end);
%IFst=Fst(15:2:135);
if nargin<1,
    S=1:size(Fst,1);
end;
if nargin<3,
    x_range=1029:2564;
    y_range=495:1940;
end;

display('loading file');

    for f=S,
    %display(f);
    disp(Fst(f).name);
   I=imread(Fst(f).name);
%   Iall(:,:,:,f)=I;
   Isub=I(y_range,x_range,:);

%   III(:,:,:,f)=Iavesub/255;
    III(:,:,:,f)=Isub;

  % clear I; clear Isub; clear Iavesub;
  clear Isub;
  %  clear Iall;
    end
    R(:,:,:)=III(:,:,1,:);
    G(:,:,:)=III(:,:,2,:);
    B(:,:,:)=III(:,:,3,:);

    for i=S,
 Rm(i)=mean(mean(R(:,:,i)));
```

```
 Gm(i)=mean(mean(G(:,:,i)));
 Bm(i)=mean(mean(B(:,:,i)));
    end

xlswrite(filename,Rm',1,'B5')
xlswrite(filename,Bm',1,'C5')
xlswrite(filename,Gm',1,'D5')
xlswrite(filename,{'R prime'},1,'E4')
xlswrite(filename,{'G prime'},1,'F4')
xlswrite(filename,{'R ratio'},1,'G4')
xlswrite(filename,{'G ratio'},1,'H4')

xlswrite(filename,{'Rm'},1,'B4')
xlswrite(filename,{'Bm'},1,'C4')
xlswrite(filename,{'Gm'},1,'D4')
xlswrite(filename,{'=(B5-(MIN($B$5:B$1999)))/((MAX($B$5:B$1999)-
(MIN($B$5:$B$1999))))'},1,'E5')
xlswrite(filename,{'=(D5-(MIN($D$5:D$1999)))/((MAX($D$5:D1999)-
(MIN($D$5:$D1999))))'},1,'F5')
xlswrite(filename,{'=(1-F2)/B2'},1,'G5')
xlswrite(filename,{'=F2/B2)'},1,'H5')
 end
```

B: MATLAB program used to analyze the spectral ruler images

APPENDIX B

Screw Mechanism Analysis

The Prototype 3 screw mechanism consists of five components and is shown in the exploded views A and B and the assembled screw is shown with the help of mid-sectional views C and D below.

1. Screw
2. Two circular rails
3. Wedge
4. Inner rod
5. Two compression springs in parallel

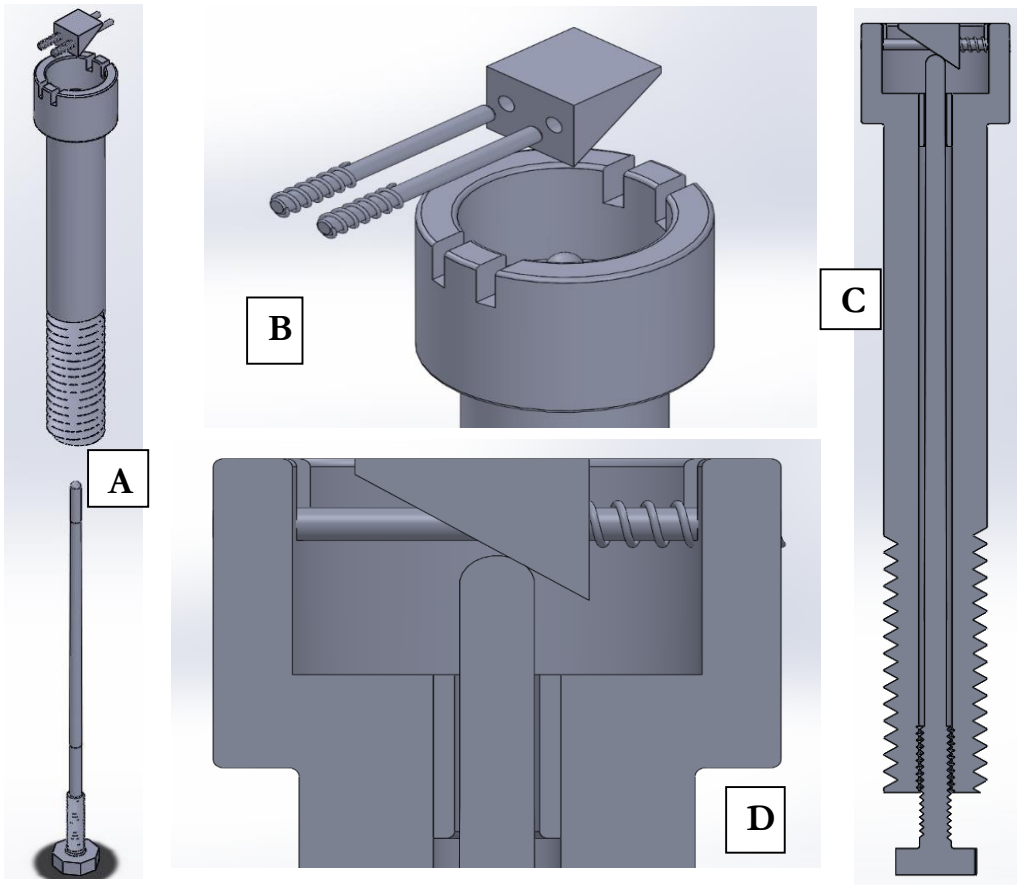

Figure B. 1: A) and B) Exploded views, C) and D) Mid-sectional views

During assembly of the wedge, circular rod and spring system, the two springs were assembled with pre compression so that the wedge comes to rest by coming in contact with the wall of the screw head as shown in Figure B. 1E. When the inner rod is assembled by threading it in, the spring is further compressed as seen in Figure B. 1D. This is the initial position before applying a tensile load of 1500 N on the screw.

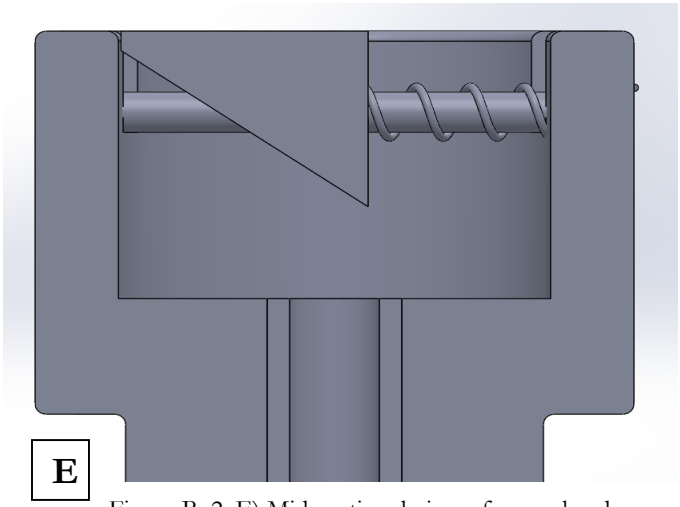

Figure B. 2: E) Mid-sectional view of screw head

Each component of the screw is considered individually and with sub-assemblies to draw the free body diagrams. The reference coordinate axes for all the free body diagrams drawn below is given by

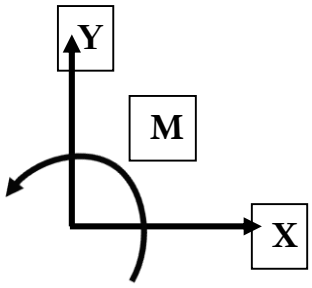

Where,

The direction of forces along X and Y as shown above are considered positive and counter-clockwise rotation of the moment is considered positive.

1. **Screw**

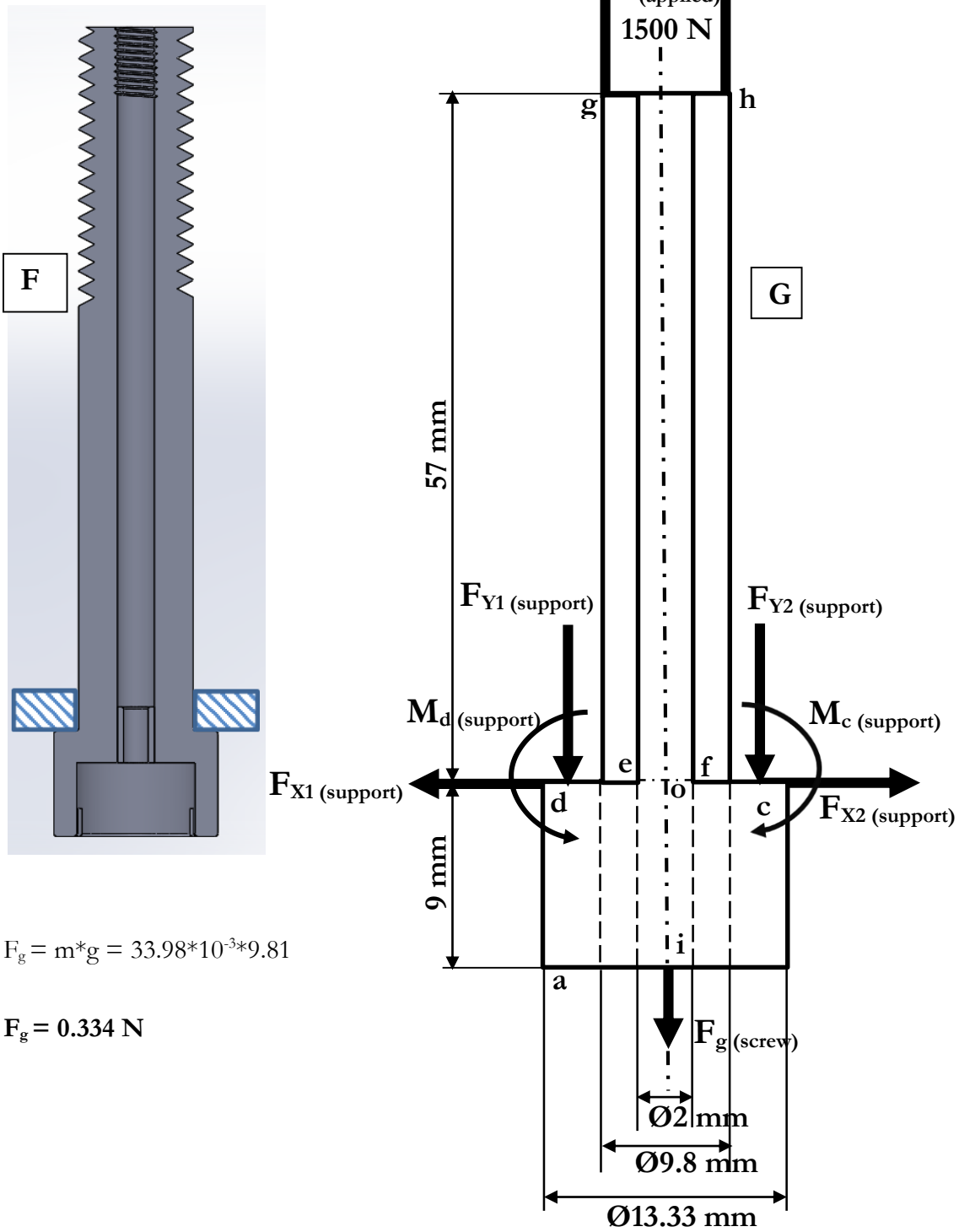

$F_g = m*g = 33.98*10^{-3}*9.81$

$F_g = 0.334$ N

Figure B. 3: F) Mid-sectional view with fixed support and G) Free body diagram of screw

The screw is fixed at the bottom surface of the head and held at the other end where the load will be applied on the screw as shown above in Figure B. 3F. The FBD of the screw is as shown in Figure B. 3G. From the FBD we can solve for the reactions at the support for an applied load of 1500 N as show below,

$$\Sigma F_X = 0, -F_{X1} + F_{X2} = 0 \Rightarrow F_{X1} = F_{X2}$$

$$\Sigma F_Y = 0, 1500 - F_{Y1} - F_{Y2} - F_g = 0 \Rightarrow F_{Y1} + F_{Y2} = 1499.67 \text{ N}$$

$$\Sigma M_o = 0, F_{Y1}*6.67 - F_{Y2}*6.67 = 0 \Rightarrow F_{Y1} = F_{Y2}$$

Therefore, $\mathbf{F_{Y1} = F_{Y2} = 749.83 \text{ N},}$

$$\mathbf{M_c = M_d =} 749.83*13.33*10^{-3} \mathbf{= 9.995 \text{ Nm}}$$

1. **Two circular rails**

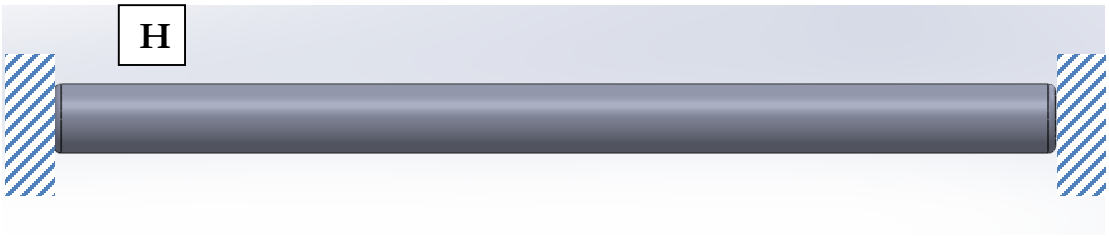

$F_g = m*g = 0.09*10^{-3}*9.81 \Rightarrow \mathbf{F_g = 0.883*10^{-3} \text{ N}}$

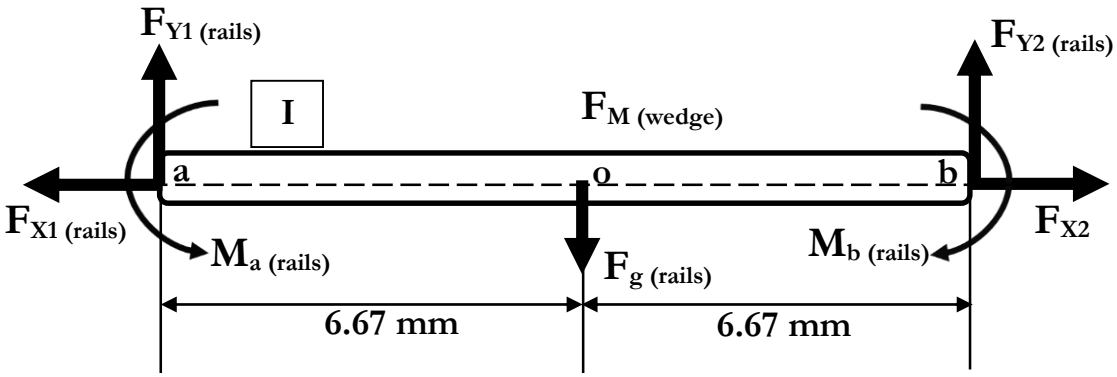

Figure B. 4: H) Circular rail with fixed support and I) Free body diagram of circular rail

Figure B. 4H shows the circular rails fixed at both ends, it is a circular beam fixed at both ends and the reactions forces at the ends are $\mathbf{F_{Y1\ (rails)}}$ and $\mathbf{F_{Y2\ (rails)}}$ as shown in the FBD in Figure B. 4I. The force due to gravity, $\mathbf{F_{g\ (rails)}}$ is acting downwards at the center of the beam as shown.

$$\Sigma F_X = 0,\ -F_{X1} + F_{X2} = 0 \Rightarrow F_{X1} = F_{X2}$$

$$\Sigma F_Y = 0,\ F_{Y1} + F_{Y2} - F_g = 0 \Rightarrow F_{Y1} + F_{Y2} = F_g = 0.883*10^{-3}\ N$$

$$\Sigma M_o = 0,\ -F_{Y1}*6.67 + F_{Y2}*6.67 = 0 \Rightarrow F_{Y1} = F_{Y2}$$

Therefore, $\mathbf{F_{Y1} = F_{Y2} = 0.441*10^{-3}\ N,}$

$$\mathbf{M_a = M_b =} 0.441*10^{-3}*13.33*10^{-3} \mathbf{= 5.88*10^{-6}\ Nm}$$

2. Wedge

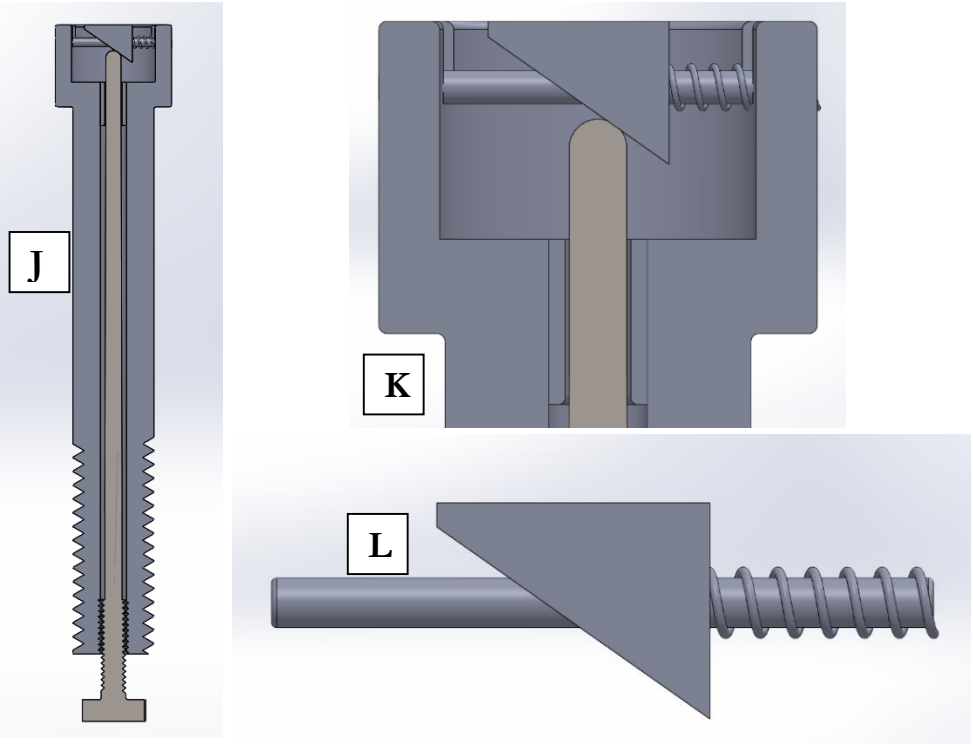

Figure B. 5: J) and K) Mid-sectional views of screw and inner rod and L) Wedge on circular rail with springs

When the tensile force is applied on the screw, the spring force displaces the wedge along the tip of the inner rod. The force in the spring is due to the compression of the spring produced by pre displacement (by rotation) of the inner rod. Figure B. 6M shows the FBD of the wedge. The reaction force due on the inner rod is at an angle and needs to be resolved into X and Y components as shown. Since the wedge is sliding on the two circular rails which constrict the upward movement of the wedge, there is a reaction force due to the rails as shown. The distributed reaction force of the rail is assumed to be acting at the center of the wedge.

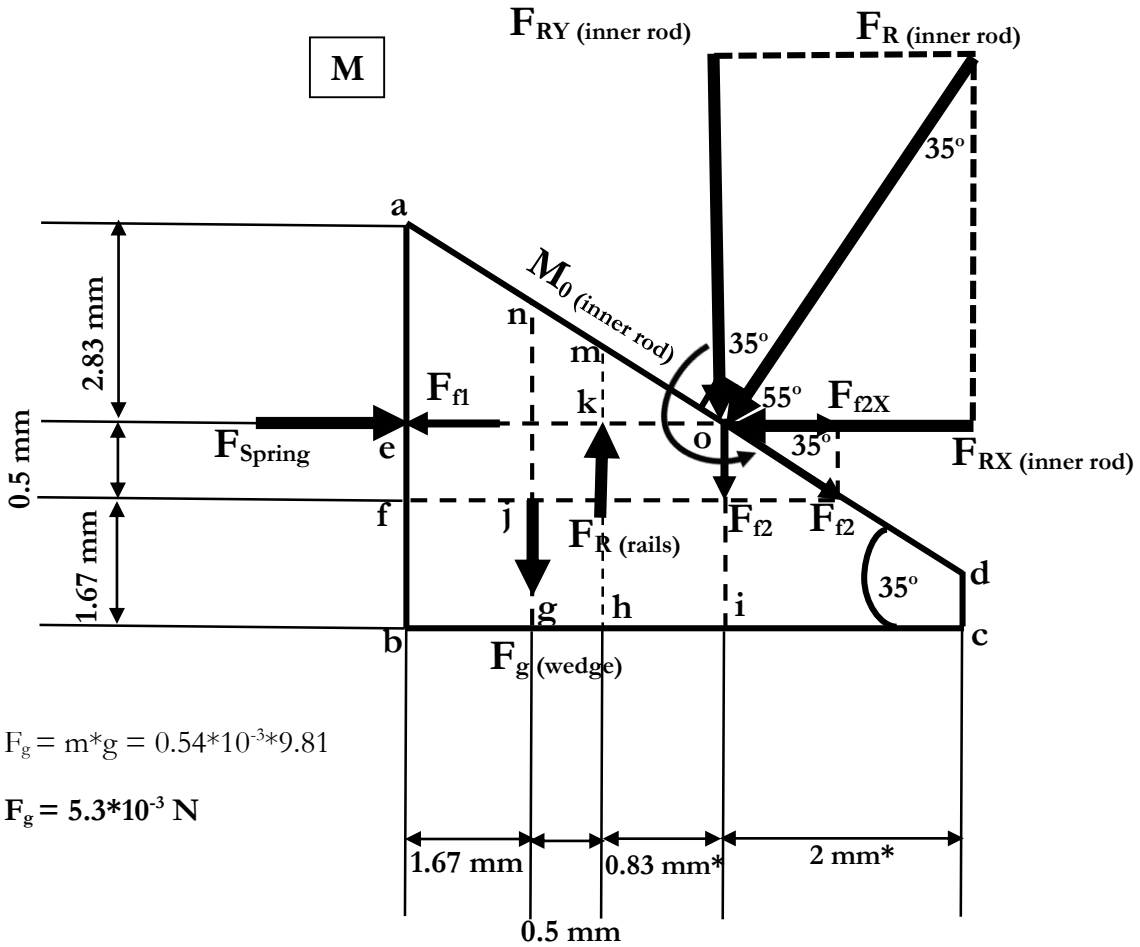

Figure B. 6: M) Free body diagram of the wedge

Where,

$F_{Spring} = (k_1 + k_2) * x$

k is the spring constant was found to be 1277.5 N/m

x is the extension in the spring

$k_1 = k_2$ as there are two springs of same spring constant in parallel

x = 200 microns = $200*10^{-6}$ m (initial pre displacement of the inner rod, the wedge compresses the spring by 200 microns)

$F_{Spring} = 2*1277.5 *200*10^{-6}$ => $\mathbf{F_{Spring} = 0.511\ N}$

$F_{R\ (inner\ rod)}$ is the reaction on the inner rod due to the wedge and its components along X and Y are $F_{RX\ (inner\ rod)}$ and $F_{RY\ (inner\ rod)}$.

F_{f1} is the friction between the wedge holes and the rails = $F_{RY\ (inner\ rod)} *\mu$ (μ is coefficient of friction between the rails and the wedge i.e. 0.61 between steel and aluminum)

F_{f2} is the friction between the wedge and the inner rod tip = $F_{R\ (inner\ rod)} *\mu$

$F_{R\ (rails)}$ is the reaction force at the rails

$M_{0\ (inner\ rod)}$ is the moment caused at the point of contact between wedge and the inner rod

From the FBD we have,

$$\Sigma F_X = 0,\ F_{Spring} - F_{f1} - F_{RX} + F_{f2X} = 0$$

$$0.511 - F_{RY\ (inner\ rod)} *\mu - F_{R\ (inner\ rod)}*\text{Cos } 55^o + F_{f2}*\text{Sin } 55^o = 0$$

$$0.511 - \mu* F_{R\ (inner\ rod)}* \text{Sin } 55^o - F_{R\ (inner\ rod)}*\text{Cos } 55^o + \mu* F_{R\ (inner\ rod)}* \text{Sin } 55^o = 0$$

$$\mathbf{F_{R\ (inner\ rod)} = 0.89\ N}$$

$$\Sigma F_Y = 0,\ -F_{f2Y} - F_{RY} - F_g + F_{R\ (rails)} = 0$$

$$-F_{f2}*\text{Cos } 55^o - F_{R\ (inner\ rod)}*\text{Sin } 55^o - 5.3*10^{-3} + F_{R\ (rails)} = 0$$

$$\mathbf{F_{R\ (rails)} = 1.05\ N}$$

$$\Sigma M_o = 0,\ M_o - F_g*1.33 + F_{R\ (rails)}*0.83 = 0$$

$$\mathbf{M_o = -\ 0.86*10^{-3}\ Nm}$$

Thus the resultant force acting on the inner rod is $F_{R\ (inner\ rod)} = 0.89$ N, the reaction force experienced by the two rails are $F_{R\ (rails)} = 1.05$ N. Finally the bending moment at point of contact is $M_o = -\ 0.86*10^{-3}$ Nm where the direction is clockwise. It can be seen that as the screw is loaded the rod moves in the upward direction along the inclined line **ad** in Figure B. 6M. So the point **o** moves closer to **m** (center of the rail) and then towards **n** (centroid of the wedge). The moment varies all along this line depending on the initial position of the point **o** which is difficult to determine. However this is controlled by the tolerance between the wedge holes and the rails. The circular tolerance zone between the circular rail and the hole in the wedge was found to be 0.19 mm (1 mm diameter holes were drilled on the wedge whereas the circular rails were 0.81 mm diameter).The bending moment may lead to tilting of the wedge and is exaggerated and shown below in Figure B. 7N.

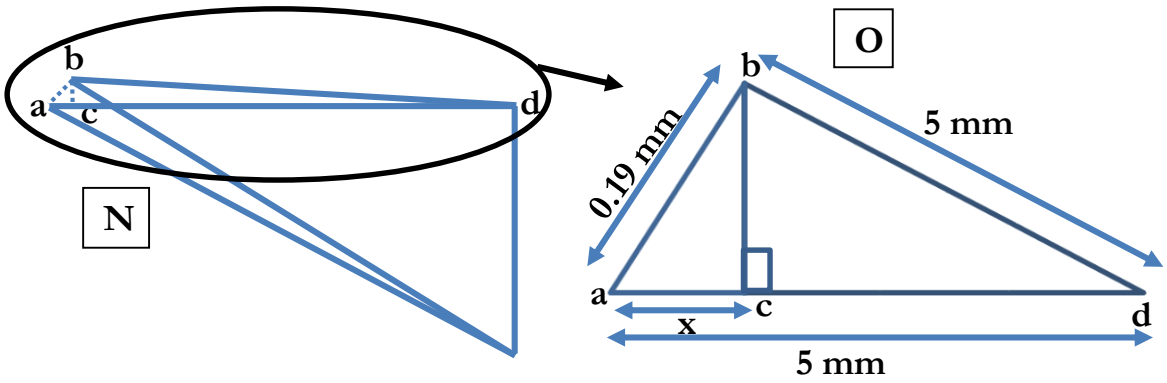

Figure B. 7: N) Inclination of wedge and O) Exaggerated view of the angle of inclination

Consider the Figure B. 7O, in triangle abc,

$$ab^2 = ac^2 + bc^2, \text{ Therefore } 0.19^2 = x^2 + bc^2 \Rightarrow bc = (0.19^2 - x^2)^{1/2}$$

Similarly from triangle bcd,

$$bd^2 = cd^2 + bc^2, \text{ Therefore } 5^2 = (5-x)^2 + 0.19^2 - x^2$$

Solving the above equation we get **x = 3.61 microns**

So 3.61 microns of horizontal movement of the wedge is lost due to the tilting of the wedge. That corresponds to 2.52 micron elongation of the screw. From simulation the elongation for 1500 N was found to be 48 micron, therefore the load required for 2.52 micron elongation of the screw is **78.9 N.** This is the amount of load that is needed to be applied to the screw before the wedge starts moving horizontally.

3. Inner rod

Figure B. 8P shows the screw and inner rod sub-assembly, Figure B. 8Q shows the inner rod and Figure B. 8R shows the FBD of the inner rod.

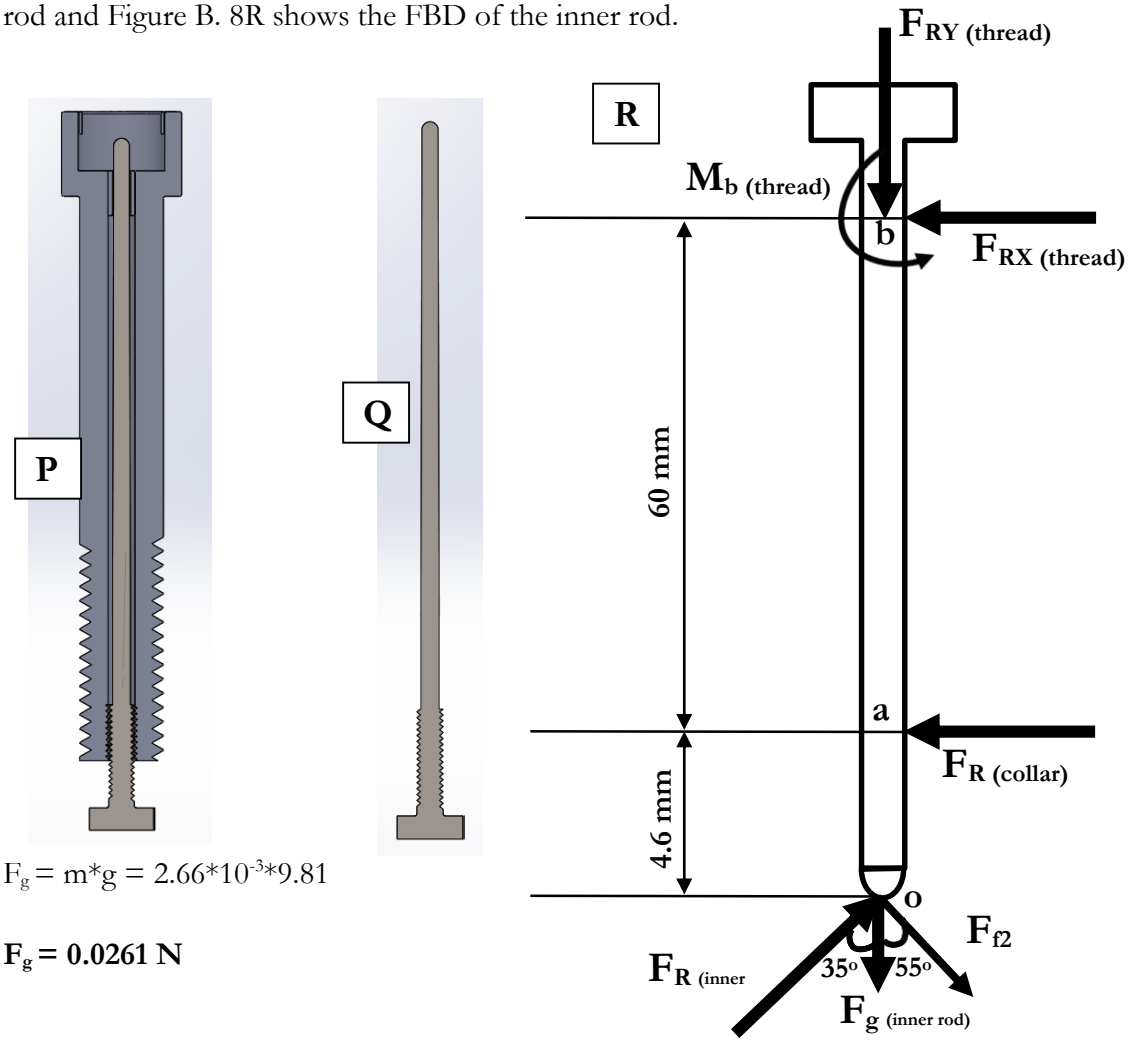

$F_g = m*g = 2.66*10^{-3}*9.81$

F_g = 0.0261 N

Figure B. 8: P) Screw and inner rod assembly view, Q) Inner rod view and R) Free body diagram of inner rod

$$\Sigma F_X = 0,\ F_{R\ (inner\ rod)}*\text{Sin } 35^o - F_{R\ (collar)} + F_{f2}*\text{Sin } 55^o - F_{RX\ (thread)} = 0$$

$$\mathbf{F_{R\ (collar)} + F_{RX\ (thread)} = 0.955\ N}$$

$$\Sigma F_Y = 0,\ F_{R\ (inner\ rod)}*\text{Cos } 35^o - F_{g\ (inner\ rod)} - F_{f2}*\text{Cos } 55^o - F_{RY\ (thread)} = 0$$

$$\mathbf{F_{RY\ (thread)} = 0.392\ N}$$

$$\Sigma M_b = 0,\ - F_{RX\ (thread)}*60 + F_{R\ (inner\ rod)}*\text{Sin } 35^o*64.6 + F_{f2}*\text{Sin } 55^o*64.6 + M_{b\ (thread)} = 0$$

$$\mathbf{-60*F_{RX\ (thread)} + M_{b\ (thread)} = -61.71}$$

$$\mathbf{M_{a\ (collar)}} = F_{R\ (inner\ rod)}*\text{Sin } 35^o*4.6 + F_{f2}*\text{Sin } 55^o*4.6 = \mathbf{4.4*10^{-3}\ Nm}$$

Since there are four unknowns and only three equations, it is similar to a statically indeterminate structure with degree 1. Using superposition method,

Deflection at **a** due to only applied loading, $\delta = PL^3/3EI$ (Deflection in a cantilever beam with point load at the free end - Euler–Bernoulli beam theory)

$$\delta_1 = (F_{R\ (inner\ rod)}*\text{Sin } 35^o + F_{f2}*\text{Sin } 55^o)*64.6^3/3EI$$

Deflection at **a** due to introduction of $F_{R\ (collar)}$ load, $\delta = Pa^2\ (3L - a)/6EI$ (Deflection in a cantilever beam with point load at a distance **a** from the fixed end)

$$\delta_2 = F_{R\ (collar)}*60^2*(3*64.6\text{-}60)/6EI$$

Deflection at any support is zero, therefore $\delta 1 = \delta_2$

Equating the above equations we get, $\mathbf{F_{R\ (collar)} = 1.7\ N}$

Substituting this in previous equations we get, $\mathbf{F_{RX\ (thread)} = -0.73\ N}$ and

$$\mathbf{M_{b\ (thread)} = 62.6*10^{-3}\ Nm}$$

$\delta_{max\ (collar)}$ = Maximum deflection of the inner rod at point **o** with collar

$$\delta_{max\ (collar)} = (F_{R\ (inner\ rod)}*\text{Sin } 35^{o} + F_{f2}*\text{Sin } 55^{o})*4.6^{3}*10^{-9}/3*E_{SS}*I_{\ (inner\ rod)})$$

$E_{SS} = 200*10^{9}\ N/m^{2}$

$I_{\ (inner\ rod)} = 3.142*(1*10^{-3})^{4}/4 = 7.855*10^{-13}\ m^{4}$

Therefore, $\boldsymbol{\delta_{max\ (collar)} = 0.2}$ **microns**

4. **Two compression springs in parallel**

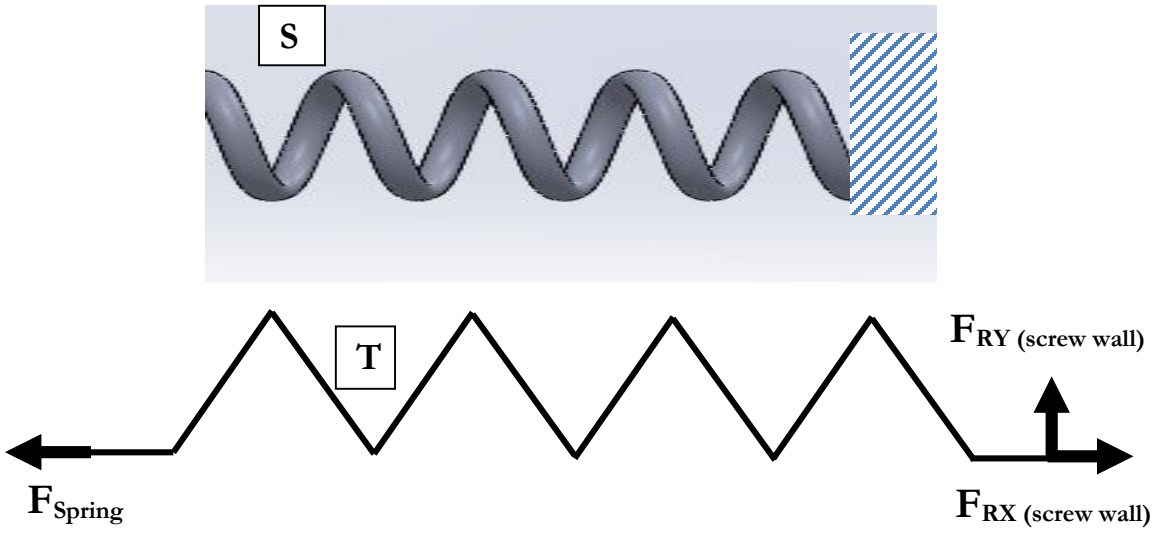

Figure B. 9: S) Spring with fixed support and T) Free body diagram of spring

The spring force F_{Spring} is acting on the wedge as shown in FBD Figure B. 9T and a reaction force $F_{R\ (screw\ wall)}$ acts on the wall of the screw where it is fixed.

$$\Sigma F_{X} = 0,\ -F_{Spring} + F_{RX\ (screw\ wall)} = 0 \Rightarrow F_{RX\ (screw\ wall)} = F_{Spring} = 0.511\ N$$

$$\Sigma F_{Y} = 0 \text{ and } \Sigma M_{Z} = 0$$

The probable causes for the hysteresis in the system are,

1. Tilting of the wedge due to the tolerance between the circular rails and holes in the wedge. The approximate value found by the calculations above show that 80 N load or 2.52 micron elongation in the screw is required to stabilize the wedge. Also from the wedge FBD it can be seen that there are two center points along which the wedge can tilt. One being the centroid of the wedge and two the midpoint of the rails. The point of contact can lie on either side of these center points. The farther away the contact point is from these center points, more will be the tilting of the wedge. Further study will look into quantifying this tilt experimentally by the use of laser points to detect the change in angle of the wedge while the screw is being loaded. Precision machining would help reduce the tolerance zone and thus provide better performance.
2. Bending of the inner rod due to the friction between the inner rod tip and the inclined surface of the wedge. The value obtained for the maximum deflection of the inner rod is 0.2 microns which might not contribute to the hysteresis seen in the system and by placing the collar closer to the wedge, it can be reduced further.

The hysteresis seen in the system indicates that the screw acts like a bistable system or toggle system where it has two defined stages which is reproducible. Though friction might be considered as a prime factor for the hysteresis, it can be seen that the hysteresis curve does not show stick-slip phenomenon throughout the cycle. This indicates that the static friction in the system is not causing the toggle effect. Also through tests conducted at various loading rates should that the hysteresis did not depend on the rate at which the load was applied on the screw. This indicates that kinetic friction in the system is also not causing the toggle effect.

Some of the probable causes for the toggle effect in the system are,

1. Spring relaxation and buckling might be one of the factors that requires the initial load before engaging and disengaging of the system. It was also observed from the hysteresis curve that at these two extreme points, there was slight drop in the color ratio before it started to increase. Further study will look into testing the screw with springs of higher stiffness.
2. One another explanation for the toggle effect might be the load transmission through the fixture to the threads of the orthopaedic screw and then from the screw threads to the inner rod threads. This is a common phenomenon seen in gears where there is slight loss in transmission between gear teeth. Further tests will be conducted by eliminating the screwing fixture and replacing it with the use of Bismuth to hold the screw and apply load.

REFERENCES

1. Ehrlich GD, Stoodley P, Ph D, et al. NIH Public Access. 2006;02418(437):59-66.

2. Oest ME, Dupont KM, Kong HJ, Mooney DJ, Guldberg RE. Quantitative assessment of scaffold and growth factor-mediated repair of critically sized bone defects. *J Orthop Res*. 2007;25(7):941-950.

3. An YH, Draughn RA. Mechanical Testing of Bone and the Bone-Implant Interface. In: *Medical*. Vol ; 1999:648.

4. Marks SC, Popoff SN. Bone cell biology: the regulation of development, structure, and function in the skeleton. *Am J Anat*. 1988;183(1):1-44.

5. Boskey AL, Posner AS. Bone structure, composition, and mineralization. *Orthop Clin North Am*. 1984;15(4):597-612.

6. Brinker, M.R., and Miller MD. *Fundamentals of Orthopaedics*.; 1999.

7. RS Lokes. Materials with structural hierarchy. *Nature*. 1993;361:511-15.

8. Heino TJ, Hentunen TA, Vaananen HK. Conditioned medium from osteocytes stimulates the proliferation of bone marrow mesenchymal stem cells and their differentiation into osteoblasts. *Exp Cell Res*. 2004;294(2):458-468.

9. Wade R, Richardson J. Outcome in fracture healing: A review. *Injury*. 2001;32(2):109-114.

10. Frost HM. Changing Concepts in Skeletal Physiology : Wolff ' s Law , the Mechanostat, and the "' Utah Paradigm ." *Am J Hum Biol*. 1998;10(July 1997):599-605.

11. Perren SM. Evolution of the internal fixation of long bone fractures. The scientific basis of biological internal fixation: choosing a new balance between stability and biology. *J Bone Joint Surg Br*. 2002;84(8):1093-1110.

12. Perren SM. Physical and biological aspects of fracture healing with special reference to internal fixation. *Clin Orthop Relat Res*. 1979;(138):175-196.

13. Gautier E, Perren SM, Cordey J, Steinemann SG, Borgeaud M, Leyvraz PF. Effect of plate position relative to bending direction on the rigidity of a plate osteosynthesis. A theoretical analysis. *Injury*. 2001;32(SUPPL. 3):14-20+78.

14. Salgar ST. Stress in first year medical students. *Int J Biomed Adv Res*. 2014;05(01):79-80.

15. Browner et al: *Skeletal Trauma, 2nd Ed, Saunders*.; 1998.

16. Lakatos AR, Editor C, Ann M. General Principles of Internal Fixation. 2014:1-16.

17. Augat P, Simon U, Liedert A, Claes L. Mechanics and mechano-biology of fracture healing in normal and osteoporotic bone. *Osteoporos Int*. 2005;16(SUPPL. 2):36-43.

18. Frost HM, Ferretti JL, Jee WS. Perspectives: some roles of mechanical usage, muscle strength, and the mechanostat in skeletal physiology, disease, and research. *Calcif Tissue Int*. 1998;62(1):1-7.

19. Parfitt AM. Osteonal and Hemi-Osteonal remodeling: The spatial and temporal framework for signal traffic in adult human bone. *J Cell Biochem*. 1994;55(3):273-286.

20. Tencer AF JK. *Biomechanics in Orthopeadic Trauma, Bone Fracture and Fixation 1st Edition. Martin Dunitz*.; 1994.

21. Tencer et al. *Biomechanics in Orthopaedic Trauma, Lippincott*.; 1994.

22. Stoffel K, Klaue K, Perren SM, Baumgart F, Fengels I. Functional load of plates in fracture fixation in vivo and its correlate in bone healing. *Injury*. 2001;32(SUPPL. 2):37-50+73.

23. Grasa J, Gómez-Benito MJ, González-Torres LA, Asiaín D, Quero F, García-Aznar JM. Monitoring in vivo load transmission through an external fixator. In: *Annals of Biomedical Engineering*. Vol 38. ; 2010:605-612.

24. Comiskey DP, MacDonald BJ, McCartney WT, Synnott K, O'Byrne J. The role of interfragmentary strain on the rate of bone healing-A new interpretation and mathematical model. *J Biomech*. 2010;43(14):2830-2834.

25. Bottlang M, Doornink J, Fitzpatrick DC, Madey SM. Far cortical locking can reduce stiffness of locked plating constructs while retaining construct strength. *J Bone Joint Surg Am*. 2009;91(8):1985-1994.

26. Fernandez M.S-B., Calderon, J.M.A., Diez, P.M.B and Segura II. Stress-separation techniques in photoelasticity: A review. *J Strain Anal Eng Des*. 2010;45:1.

27. Guenther RD. *Modern Optics, 1st Edition, New York, Wiley*.; 1990.

28. McKelvie J. Moiré strain analysis: an introduction, review and critique, including related techniques and future potential. *J Strain Anal Eng Des*. 2005;33(2):137-151.

29. Han B, Post D, Ifju P. Moire Interferometry For Engineering Mechanics: Current Practices and Future Developments. *J Strain Anal*. 2001;36 :101-117.

30. He X. Phase-shifting analysis in moiŕe interferometry and its applications in electronic packaging. *Opt Eng*. 1998;37(5):1410.

31. Fleming BC, Beynnon BD. In vivo measurement of ligament/tendon strains and forces: A review. *Ann Biomed Eng*. 2004;32(3):318-328.

32. French PJ. Polysilicon: A versatile material for microsystems. *Sensors Actuators, A Phys*. 2002;99(1-2):3-12.

33. Practical strain measurements. (2012). Retrieved from www.vtiinstruments.com/Practical-Strain-Measurements.aspx.

34. Joshi SG, Pathare RG. ULTRASONIC INSTRUMENT FOR MEASURING BOLT STRESS. *Ultrasonics*. 1984;22(6):270-274.

35. Heyman JS. *A CW Ultrasonic Bolt-Strain Monitor. Experimental Mechanics*.; 1977.

36. Lake J. Development and Verification of a Test System to Quantify Strain of an Optical Displacement Indicator and the Design of a Strain Indicating Prototype. 2013.

37. Wang F, Raval Y, Chen H, Tzeng TRJ, Desjardins JD, Anker JN. Development of luminescent pH sensor films for monitoring bacterial growth through tissue. *Adv Healthc Mater*. 2014;3(2):197-204.